Simulated Hail Ice Mechanical Properties and Failure Mechanism at Quasi-Static Strain Rates

Jonathan M. Swift

A Thesis
submitted in partial fulfillment of the
requirements for the degree of

Master of Science in Aeronautics and Astronautics

University of Washington
2013

Committee:
Paolo Feraboli
Robert Breidenthal

Program Authorized to Offer Degree:
Aeronautics and Astronautics

Executive Summary

Hail is a significant threat to aircraft both on the ground and in the air. Aeronautical engineers are interested in better understanding the properties of hail to improve the safety of new aircraft. However, the failure mechanism and mechanical properties of hail, as opposed to clear ice, are not well understood. A literature review identifies basic mechanical properties of ice and a failure mechanism based upon the state of stress within an ice sphere is proposed.

To better understand the properties of Simulated Hail Ice (SHI), several tests were conducted using both clear and cotton fiber reinforced ice. Pictures were taken to show the internal crystal structure of SHI. SHI crush tests were conducted to identify the overall force-displacement trends at various quasi-static strain rates. High speed photography was also used to visually track the failure mechanism of spherical SHI. Compression tests were done to measure the compression strength of SHI and results were compared to literature data. Fracture toughness tests were conducted to identify the crack resistance of SHI. Results from testing clear ice samples were successfully compared to previously published literature data to instill confidence in the testing methods. The methods were subsequently used to test and characterize the cotton fiber reinforced ice.

Table of Contents

List of Figures

List of Tables

I. Introduction

Weather is a significant influence on an aircraft's operating environment. As aircraft become more common, it becomes increasingly important for engineers to account for severe weather to protect people and goods. One well documented weather related threat to aircraft is hail. Hail is a form of precipitation associated with thunderstorms. Under the correct conditions, the moisture in a thunderstorm can freeze into ice. Hail is a layered accumulation of ice and trapped air greater than 5mm in size [1]. Though the formation process is not completely understood by meteorologists, it is believed that hail forms when updrafts and downdrafts push ice crystals between freezing and nonfreezing layers in a thunderstorm. Additional moisture adheres to the crystal while the surface repeatedly freezes and melts. This changes the relative air content of the ice crystals, creating a layered, onion-like cross section. The ice then falls as hail when the internal winds are no longer strong enough to keep it airborne [2]. Depending upon the conditions, hail can vary widely in size and density, and presumably, in mechanical properties.

Though not every thunderstorm produces hail, they do occur more frequently in certain parts of the world, as can be seen in Figure 1. Engineers need to account for two types of hail strikes: during flight and on the ground.

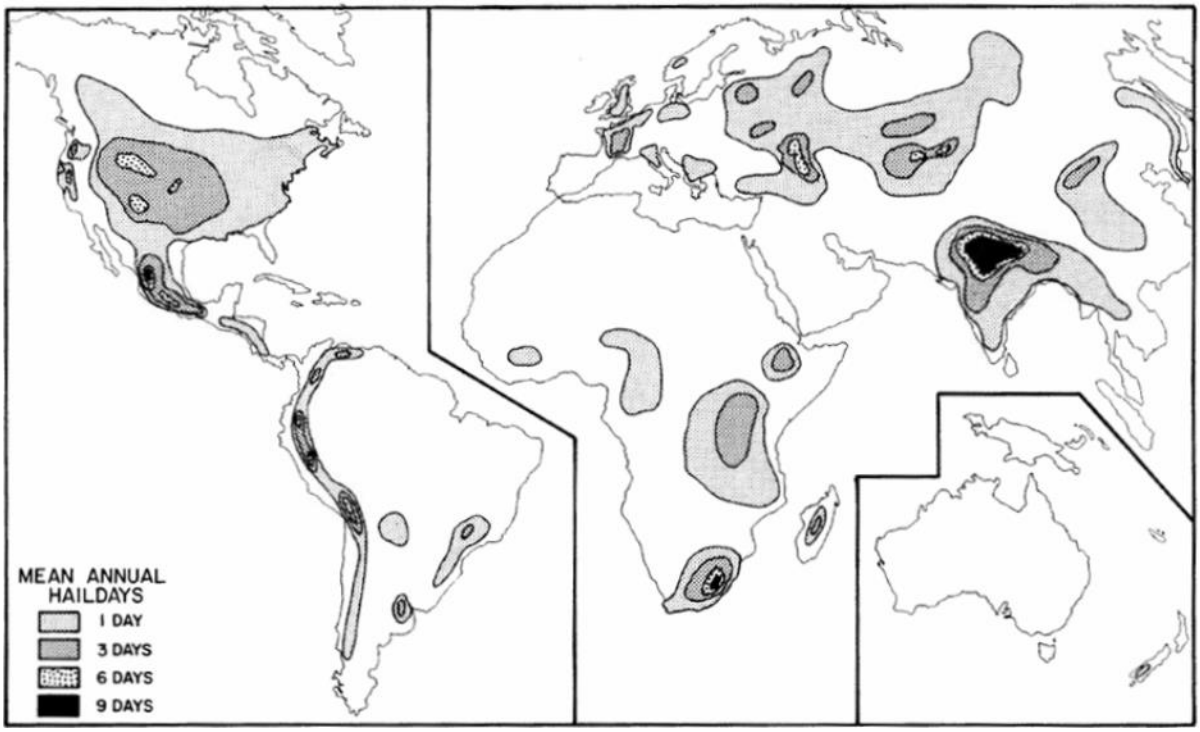

Figure 1: Global Hailstorm Frequency [3]

Though pilots actively avoid the dangerous weather systems responsible for creating hail, hail strikes during flight can and do occur. These strikes tend to impact the leading edges of the aircraft at flight velocities, and may put the crew and passengers at risk by seriously damaging flight systems. Two incidents are sufficient to illustrate the threat. The first occurred on 7 May 1998 near Calhoun, Georgia [4]. The crew of AirTran Airlines Flight 426 attempted to fly through a gap in a line of thunderstorms when the airplane entered an area with severe turbulence and hail. The crew made an emergency landing at the Chattanooga Metropolitan Airport with a passenger and flight attendant seriously injured. The DC-9 aircraft landed with a partially shattered windshield, missing radome, and damage to the pitot system, wings, tail, and engines. Pictures of the damage are shown in Figure 2.

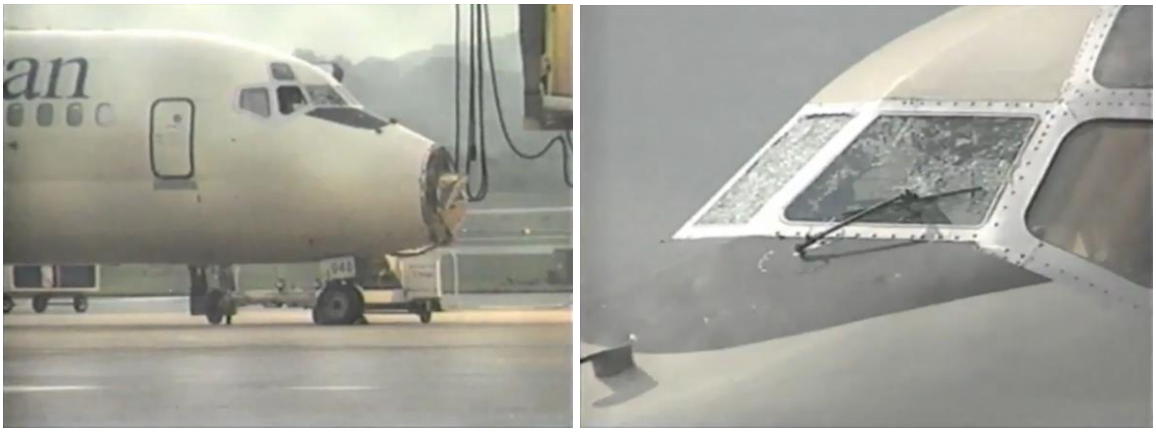

Figure 2: DC-9 Hail Strike Damage, 7 May 1998 [5]

The second occurred on 14 August 2003 on EasyJet Airlines Flight 903 near Geneva, Switzerland [6]. As reported by the Swiss Aircraft Accident Investigation Bureau (BFU), the Boeing 737 encountered a hailstorm shortly after takeoff, forcing the crew to return to Geneva for an emergency landing. The hail severely damaged the radome, windshield, and leading edges of the horizontal and vertical surfaces, as can be seen in Figure 3.

Figure 3: Boeing 737 Hail Strike Damage, 14 Aug 2003 [7]

Aircraft can also be damaged by hail on the ground. In these cases, the hail tends to strike perpendicular to the aircraft surfaces, such as on the top of the wing or fuselage, at much lower velocities than experienced during flight. Hailstorms can shut down airport operations and

may damage many aircraft. This happened on 3 April 2012 at the Dallas-Fort Worth International Airport when hail damaged over 100 aircraft [8]. Storms like that disrupt travel and prompt unscheduled inspections and repairs on damaged aircraft, increasing costs for both airlines and passengers.

This hail threat grows due to the increasing use of composite materials in aircraft. The latest passenger airliners from Boeing and Airbus are increasingly made of carbon fiber reinforced plastics (CFRP). For example, both the Boeing 787 [9] and Airbus A350 XWB [10] are approximately 50% composite materials by weight. While using composites in aircraft structures offer numerous production and performance advantages over traditional metals, it must be understood that composites are damaged and fail differently than metals.

Currently, there are few regulations which deal with mitigating the threat specifically due to hail strikes for metallic, let alone composite aircraft. In the United States, the regulations governing aviation are found in the Code of Federal Regulations (CFR), Title 14: Aeronautics and Space, Chapter 1: Federal Aviation Administration (FAA). Parts 23 and 25 specifically deal with the airworthiness of small commuter and large transport class aircrafts, respectively [11]. Part 25 does not directly address the impact of hail strikes on aircraft structures, though section 25.571 states, "An evaluation of the strength, detail design, and fabrication must show that catastrophic failure due to fatigue, corrosion, manufacturing defects, or accidental damage, will be avoided throughout the operational life of the airplane" [12]. This includes hail strike damage. Section 25.773 specifically mentions that an aircraft must be able to safely land in the event of hail damage to the windscreen [13]. ASTM Standard F320-10 [14] outlines a test procedure for meeting the requirements outlined in section 25.773 and will be referenced frequently in this paper simply as ASTM F320.

Unfortunately, the mechanical properties of actual hailstones are not well understood. While many basic properties, such as size and density, have been studied, it is difficult to obtain hailstones suitable for testing. Most hail research for aeronautical applications has split along two different approaches. In the first, researchers assume that hail has the same mechanical properties as solid ice. Thus, this research focuses on studying the properties and creating models of ice, as distinct from hail, for experiments under conditions in which aircraft operate. In the second, researchers use the test method outlined in ASTM F320, which assumes that hail is less dense and tougher than clear ice. Cotton is added to the test ice specimens at 12% concentration by mass to approximate these two properties. Unfortunately, until the mechanical properties of actual hailstones are determined, neither approach can be verified. In this paper spherical test specimens representing hail will be referred to as Simulated Hail Ice (SHI). SHI can consist of either clear ice (clear-SHI) or cotton fiber reinforced ice (cotton-SHI).

This thesis consists of several related parts. The first is to conduct a literature review on the mechanical properties of ice and the failure mechanism of spheres under compression. Clear-SHI samples were tested for comparison to literature data to establish confidence in the testing methods. The same methods were subsequently used to test cotton-SHI outlined in ASTM F320 which may more accurately model the hail threat to aircraft. It should be noted that there is no previously published data on the mechanical properties of cotton-SHI. Testing focused on the most important properties related to the failure mechanism of spheres under compression.

II. Background

A. Mechanical Properties of Ice

The study of ice plays a significant role in many diverse engineering disciplines. Ice is a part of professional winter sports, influences the design of Artic oil drilling platforms, and can destroy electrical power lines. The study of ice from a mechanical engineering standpoint effectively began during World War Two when Geoffrey Pyke proposed using icebergs as natural aircraft carriers [15]. While there has been significant research into ice properties, little has focused on hail and even less on fiber reinforced ice.

As water freezes into ice, the molecules arrange into an ordered, crystalline form. The crystalline structure of ice can vary depending upon the freezing conditions. For example, Artic sea ice tends to consist of columnar shaped crystals while the crystals in glacial ice tend to be randomly arranged [16]. Previous research indicates that ice with relatively small, randomly arranged crystals is approximately isotropic. For this kind of ice, the basic mechanical properties are shown in Table 1.

Table 1: Basic Properties of Isotropic Ice, 3°F (-16°C) [17, 18]

Property	Units	Value
Young's Modulus, E	Nm^{-2}	9.33×10^{9}
Compressibility, K	$N^{-1}m^{2}$	112.4×10^{-12}
Bulk Modulus, B	Nm^{-2}	8.90×10^{9}
Shear Modulus, G	Nm^{-2}	3.52×10^{9}
Poisson's Ratio, ν	n/a	0.325
Density	$kg\ m^{-3}$	917

Three other important properties are the compression strength, tensile strength, and fracture toughness. For ice, these properties are strain rate dependent and cannot be quantified by a single value. At low strain rates, ice behaves in a ductile manner in both tension and

compression. When loads are slowly applied, creep dominates and the ice crystals deform [19]. As the strain rate is increased, the ice eventually reaches a point where it cannot deform fast enough without cracking. This is known as ductile-brittle transition point for ice. Beyond this point, ice behaves in a brittle manner and is characterized by being unable to carry additional load after fracturing. Graphically, this transition point is shown in general terms in Figure 4.

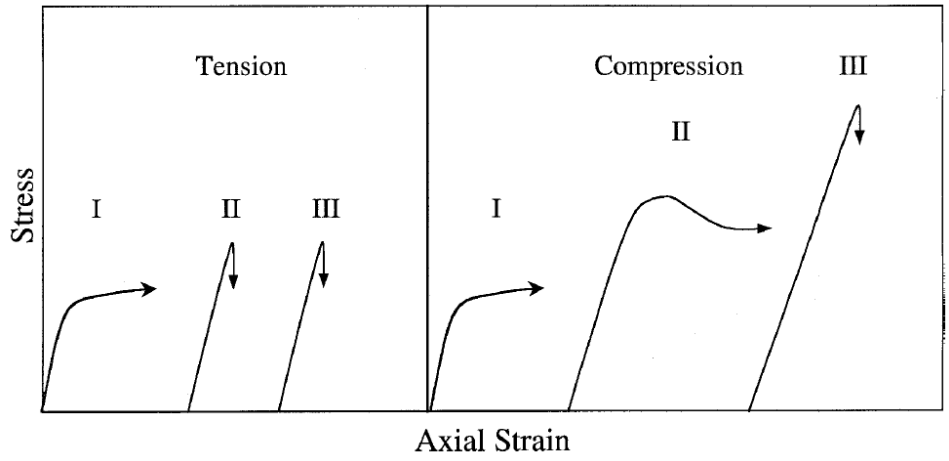

Figure 4: Clear Ice Stress-Strain Behavior -
Curves I, II, III Denote Low, Medium, High Strain Rates, Respectively [16]

At low strain rates (Curve I), the ice continues to carry load beyond the initial linear-elastic region. At high strain rates (Curve III), the ice undergoes brittle fracture, marked by the sharp peak in the curve. For both tension and compression strength testing, the strength increases with increasing strain rate until the transition point when the strength plateaus. At extremely high strain rates, such as would be experienced by hail, the compression strength continues to increase, as seen in Figure 5. However, the tensile strength of ice is not as strain rate sensitive as compression strength. It stays relatively constant in between the quasi-static strain rates 10^{-7} – 10^{-1} 1/s, though there is some evidence to suggest that tensile strength increases at high strain rates [20].

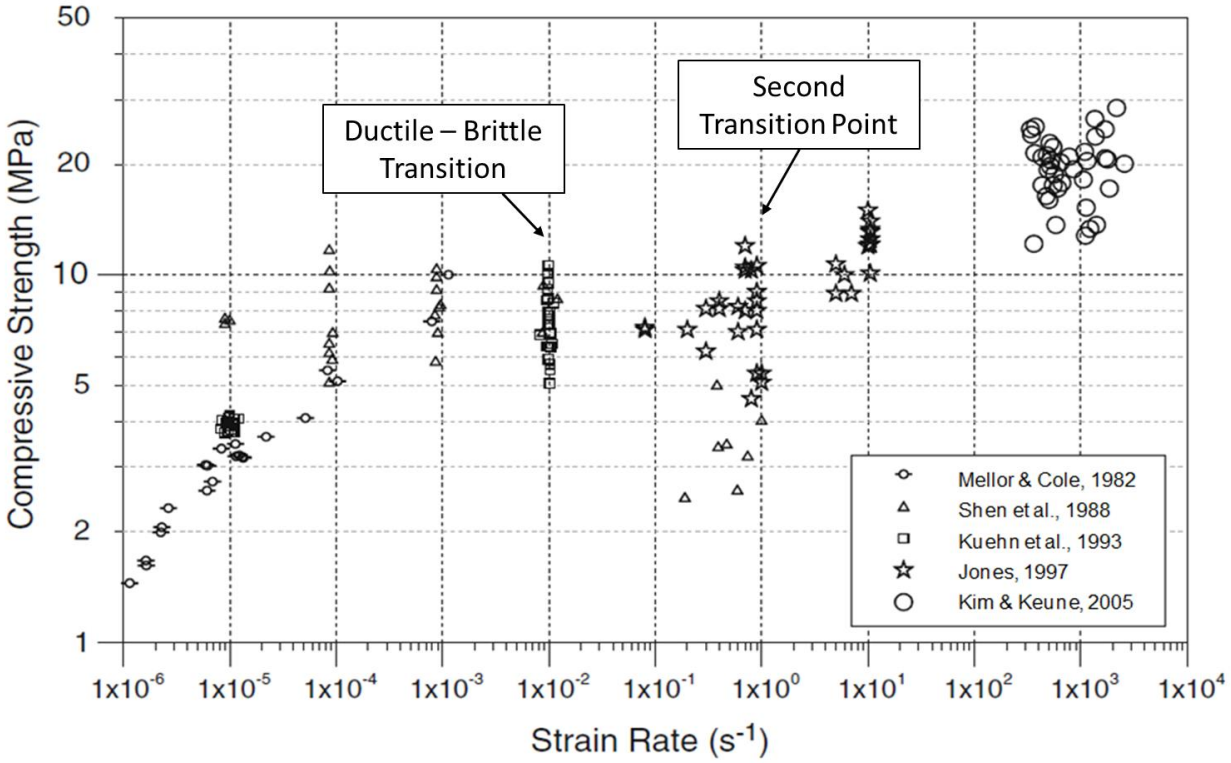

Figure 5: Ice Compressive Strength Compilation [21]

There are two main ways to measure the compression strength of ice. The first is the direct method by crushing a cylinder of known size [22]. This can be an effective and accurate method if care is taken to ensure ideal testing conditions, such as by controlling the temperature and specimen dimensions. Another method used is a Split Hopkinson Pressure Bar (SHPB) [23]. In this method, an ice sample is hit by a striker bar, causing pressure waves to travel through the ice. These pressure waves are then measured and converted to compression strength. While this method requires specialized equipment, it is relatively easy to obtain high strain rate measurements.

There are several ways to measure the tensile strength of ice, as outlined by Schulson [24]. Because ice is a more difficult to work with than metals, there have been several direct and indirect methods used. The ring and Brazil test methods indirectly measure the tensile strength

by crushing a cylinder in such a way as to induce tensile loads. A major problem with these methods is the varying stress state. Bending tests are another indirect method, but additional research indicates that the flexural strength of ice is higher than the tensile strength [24]. Though more difficult to set up, direct tensile tests give the most reliable results overall.

A summary of the tensile strength in between the strain rates 10^{-7} – 10^{-1} 1/s is shown in Figure 6. Comparing the tensile and compression strength data suggests that, as a general rule of thumb, the tensile strength is about an order of magnitude less than the compression strength.

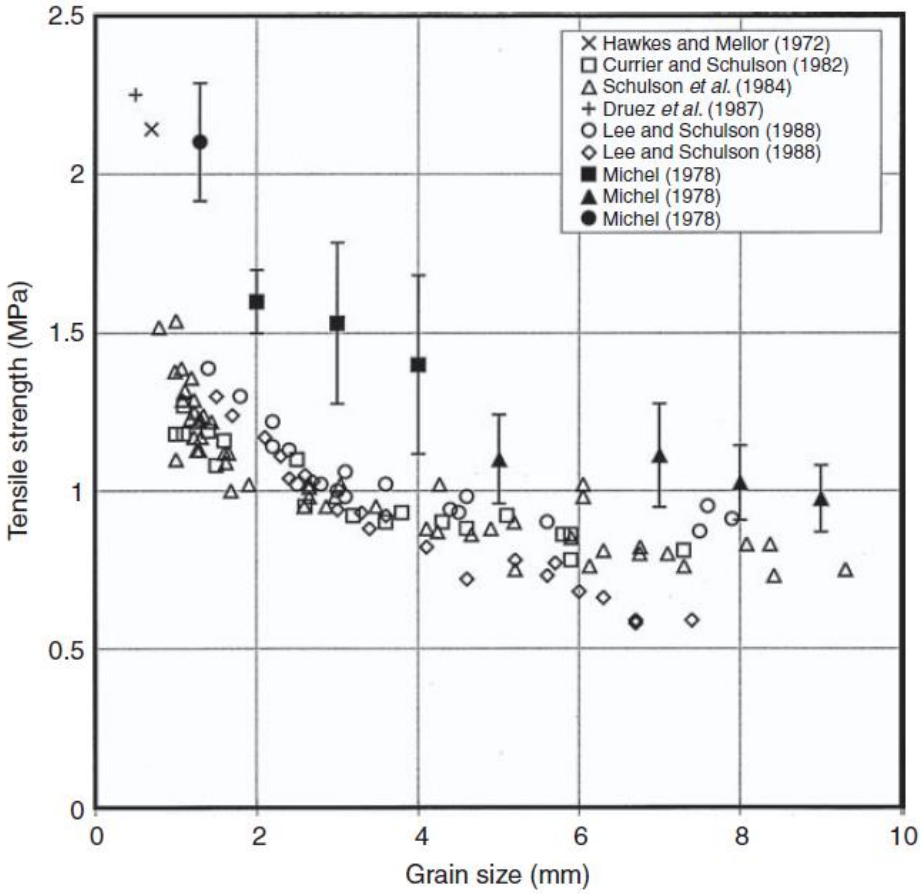

Figure 6: Ice Tensile Strength Data Compilation, 14°F (-10°C) [20]

The fracture toughness of ice is another important property to determine. Fracture toughness measures a material's ability to resist the formation and propagation of cracks. There

are three types of crack propagation, shown in Figure 7. Mode I, or crack opening occurs because of tensile forces. In most situations, Mode I fracture dominates the overall crack propagation of ice [25].

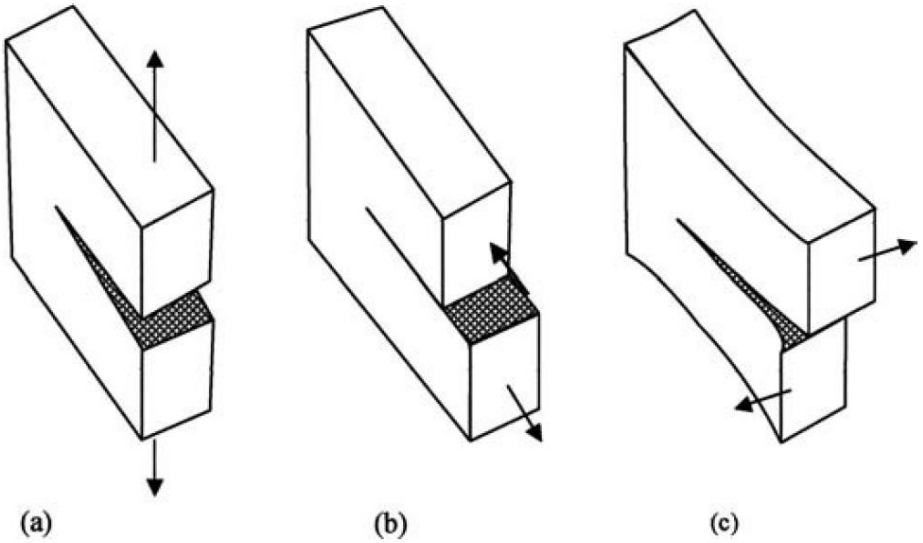

Figure 7: Types of Crack Propagation –
a) Mode I, Crack Opening b) Mode II, Crack Sliding c) Mode III, Crack Tearing [25]

There are several ways to measure fracture toughness. These include three and four point notched beam bend tests, double-cantilever beams, and circumferentially notched tensile bars. In all of these methods, a test sample with a starter crack is placed under load, causing the crack to propagate. With the correct setup, all methods are regularly used in ice testing [26].

Like compression and tensile strength, the Mode I fracture toughness, or K_{IC}, of ice is rate dependent. When under small loading rates, the ice in the notch deforms before breaking. This increases the apparent fracture load. However, at a high enough load rate, the ice is not able to deform before fracturing. Above this critical load rate, the K_{IC} value remains constant. This trend can be seen in Figure 8.

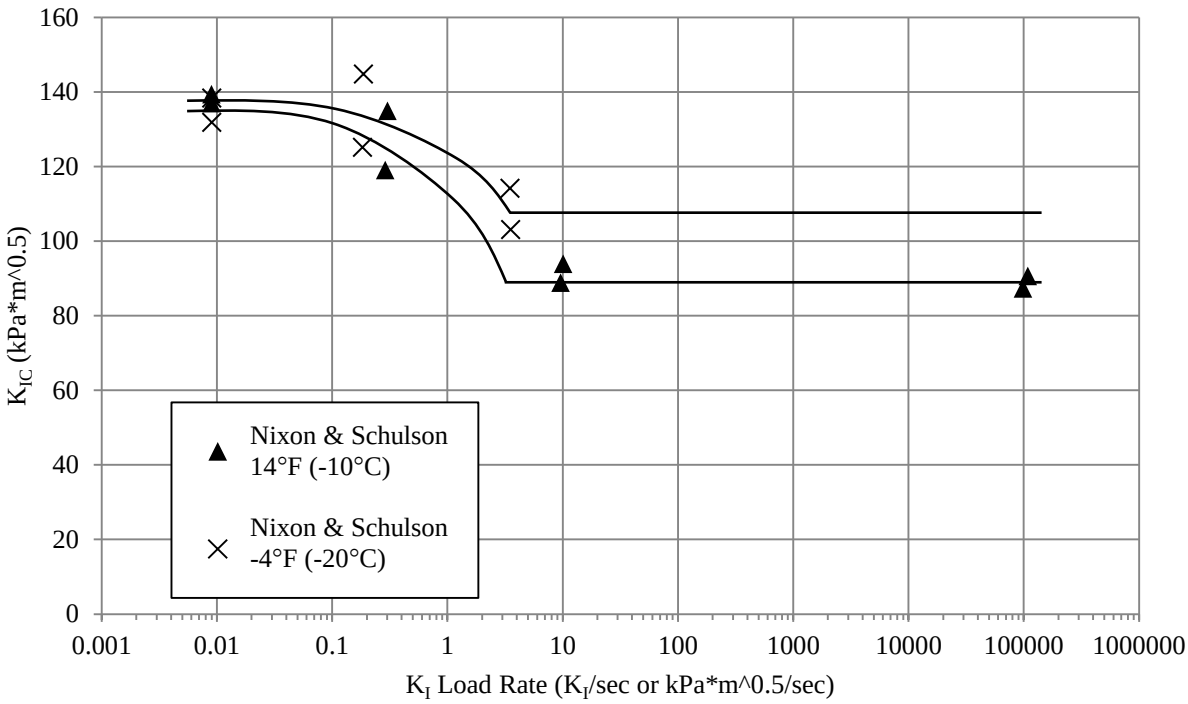

Figure 8: Clear Ice K_{IC} Rate Dependence [27]

As with compression and tensile strength, there is relatively high scatter in the published data on the fracture toughness of ice. However, the general trends suggest that fracture toughness is relatively independent of temperature. A compilation of data found within literature is shown in Figure 9.

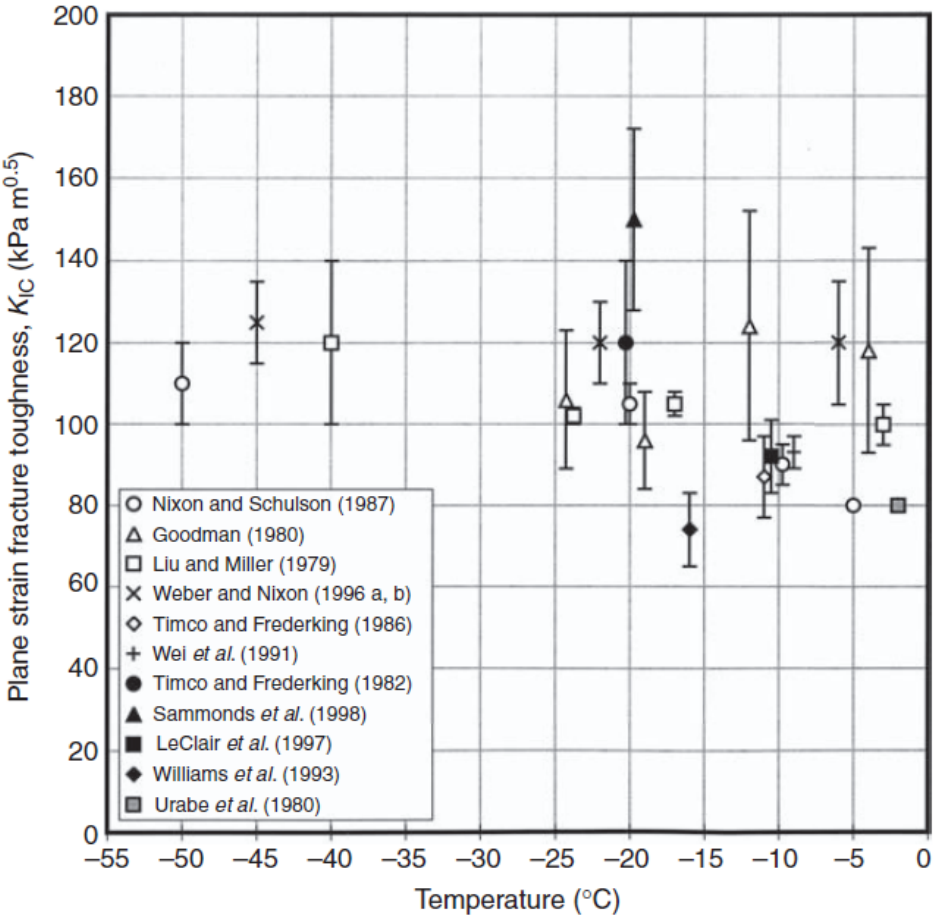

Figure 9: Clear Ice K_{IC} Data Compilation [26]

In his experiments on making an aircraft carrier from ice, Pyke added wood fibers to the ice to improve the tensile strength and fracture toughness. However, there has been little research towards identifying the effects wood based fibers have on ice [28]. In particular, there has been no research on how cotton fibers influence the strength or toughness of ice.

While basic mechanical properties are known and documented for solid ice, it is unknown if or how they are different for hail. One known difference is density. Because hail may contain trapped air bubbles within the layers of ice, depending on the atmospheric conditions within the thunderstorm at the time of formation, the density is less than solid ice.

The air bubbles give the hail a milky, optically opaque look. A compilation of recorded hail densities is shown in Figure 10.

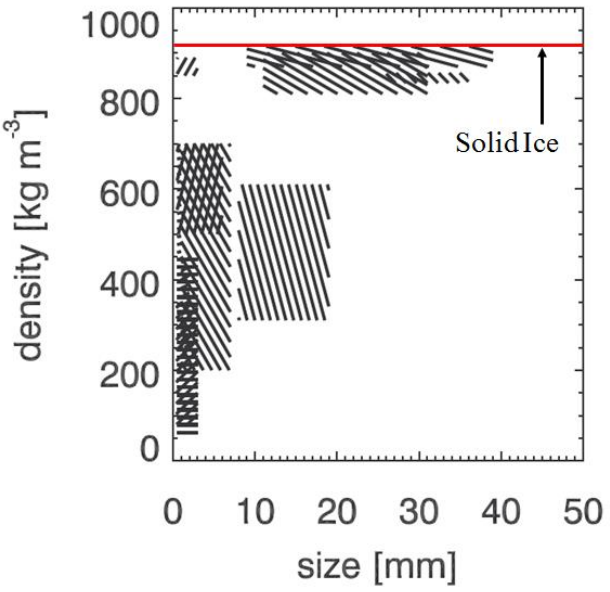

Figure 10: Hail Density Compilation [29]

B. Stress Within a Sphere Under Compression

Understanding how spherical ice fails during an impact begins with knowing the state of stress within a sphere under compression. While studying the mechanical properties of rocks, Hiramtsu and Oka [30] determined an analytical solution for the state of stress for a perfectly brittle sphere under compression. A graphical reproduction of their general solution, looking along the z-axis running directly between two point loads, is shown in Figure 11.

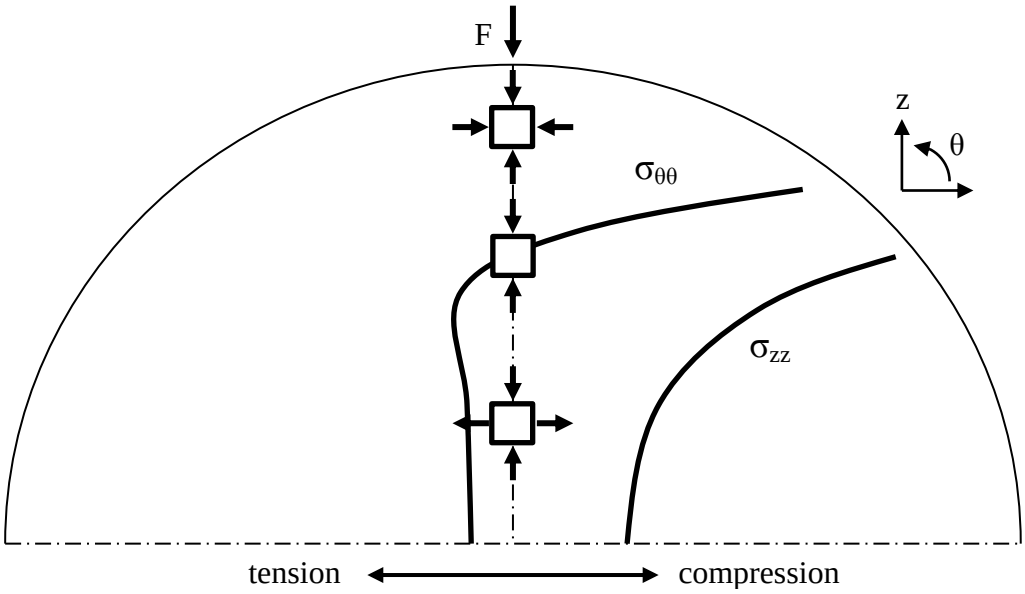

Figure 11: Radial and Hoop Stresses Along z-axis in Sphere (Half Sphere Shown) under Compression, with Stress Elements [30]

As can be seen, near the outside edge of the sphere, a stress element is under compressive stresses along both principle directions. However, stress elements near the center experience both compressive and tensile stresses. Therefore, Hiramatsu and Oka predicted that a sphere could fail in three ways: tension fracture in the center of the sphere, compression fracture near the loading points, compression fracture throughout the plane of loading, or some combination of the three. Because they were working with rocks, which are stronger in compression than tension, they assumed that tension fracture would dominate the overall failure mode.

Making several other assumptions to simplify the analysis, they proceeded to develop an analytical solution for estimating the tensile strength of a perfectly brittle sphere. The simplified solution is

$$\sigma_t \cong 1.4\frac{F_0}{2\pi a_0^2} \cong 0.9\frac{F_0}{d_0^2} \quad (1)$$

where σ_t is the estimated tensile strength, F_0 is the failure load, and $2a_0$ or d_0 is the distance between the contact surfaces at the moment of failure. This model assumes a sphere made of a perfectly brittle, isotropic material with minimal contact area between the sphere and the compression plates. As such, this formula should only be used as a quick estimate for the tensile strength. Several studies have sought to improve upon this analytical solution [cf. 31-35] but most do not significantly differ from the above. Additional experimental studies have tended to confirm the validity of this equation [34].

Russell and Wood [35] developed an analytical solution for the compression strength of a perfectly brittle sphere. Using the Poisson ratio $\nu = 0.325$, the previously mentioned value for clear ice, the estimated compression equation reduces to

$$\sigma_c \cong 0.44 \frac{F_0}{\pi a^2 \sin^2(\theta_0)} \tag{2}$$

using the dimensions shown in Figure 12.

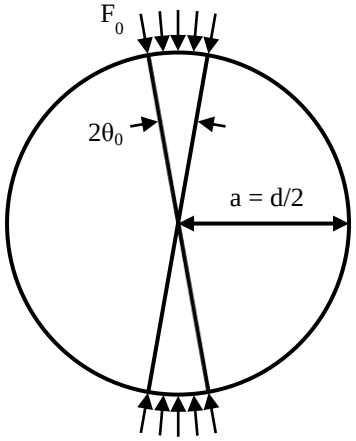

Figure 12: Compression Estimate Parameter Diagram

These equations may be used to estimate the compression or tensile strength of a perfectly brittle material.

III. Specimen Production

A. Simulated Hail Ice Production

Because it is difficult to find and test natural hailstones, the majority of research has focused on characterizing simulated hail ice (SHI). Currently, there are two main types of SHI used for testing in both academia and industry: clear and cotton reinforced ice, neither of which exactly represents natural hailstones.

To produce SHI, a mold was created out of acrylonitrile butadiene styrene (ABS) using a STRATASYS FORTUS 400mc 3D printer. The mold contained cavities allowing the creation of 0.5, 1.0, 2.0, and 2.5 inch (12.7, 25.4, 50.4, 63.5 mm, respectively) diameter ice spheres. It allowed the repeatable production of multiple specimens at any one time. The mold consists of two mirrored halves sealed together with bolts and wing nuts. To prevent leaks, a 1/32 inch rubber gasket fits in between the halves. Vent tubes, one connected to each cavity, were used to fill the specimens with water and cotton and give room for water expansion during freezing. A picture of the mold with sample specimens is shown in Figure 13.

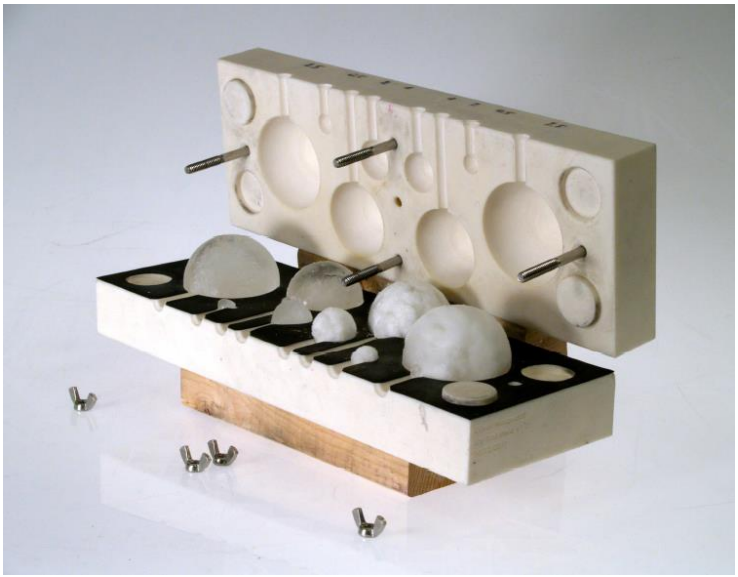

Figure 13: SHI Mold [36]

The ASTM F320 [14] uses SHI made of balls with approximately 12% cotton filler by mass. The cotton decreases the density and toughens the SHI to better simulate natural hailstones. For testing, varying amounts of cotton filler were used in the SHI as shown in Table 2. Note that clear and ASTM F320 Standard samples are indicated in the "Notes" column of the table, and that there is a 1:1 relationship between the percent of cotton by mass and the cotton fiber volume content.

Table 2: SHI Cotton Fill Amounts

Specimen Description	Diameter	Diameter	Total Mass	Cotton	Cotton	Fiber Volume	Notes	Water
	[in]	[mm]	[g]	[g]	[% Mass]	[%]		[ml]
0.5 in (12.7 mm)/ clear	0.5	12.7	1.2	0	0	0	clear	1.2
0.5 in (12.7 mm)/ cotton				0.14	14	14	ASTM	1
1.0 in (25.4 mm)/ clear	1	25.4	9	0	0	0	clear	9
1.0 in (25.4 mm)/ cotton				1	12	12	ASTM	8
2.0 in (50.8 mm)/ clear	2	50.8	66	0	0	0	clear	66
2.0 in (50.8 mm)/ 4g				4	6	6		62
2.0 in (50.8 mm)/ 8g				8	12	12	ASTM	58
2.5 in (63.5 mm)/ clear	2.5	63.5	128	0	0	0	clear	128
2.5 in (63.5 mm)/ 2g				2	1.5	1.5		126
2.5 in (63.5 mm)/ 4g				4	3	3		124
2.5 in (63.5 mm)/ 6g				6	4.5	4.5		122
2.5 in (63.5 mm)/ 8g				8	6	6		120
2.5 in (63.5 mm)/ 15.6g				15.6	12	12	ASTM	113

To create the SHI, first the required amount of cotton is weighed out from standard cotton balls. The balls are then unrolled and fluffed to help ensure an even distribution inside the cavities. Regular tap water is added into the closed mold cavities using a medical syringe. No effort is made to "purify" the water. The cotton and water are alternately added through the vent holes to prevent dry spots in the cotton and to help ensure an even distribution. When filled, the entire mold is frozen overnight at -7°F (-22°C).

Because the SHI tends to freeze to the mold cavities, the mold needs to be warmed to facilitate removal. Placing the entire mold in a container of lukewarm tap water for 5 minutes allows for easy removal without breaking or cracking the specimens. Care must be taken to ensure that this water does not enter the vent tubes. The SHI is stored in a sealed plastic bag in the freezer until ready for testing.

The SHI specimens tend to have a cloudy center with clear ice along the outside. There also tends to be a ring or disc of cloudy ice which forms along the boundary of the two halves of the matched mold. This suggests that the ice freezes from the outside in, with the water along the mold seam and rubber gasket freezing slower than the rest of the specimen. Pictures of both the clear and cotton-SHI are shown in Figure 14.

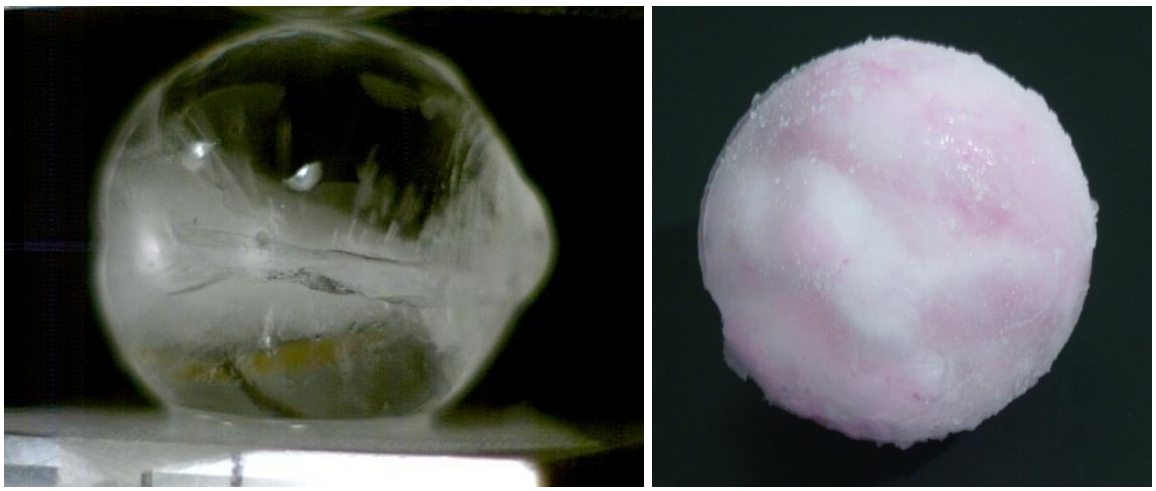

Figure 14: Clear and Cotton-SHI Pictures

B. SHI Disc Production

Discs of ice derived from spherical SHI were used for photographing the internal crystal structure within the SHI. Two clear-SHI samples were prepared and frozen as normal. When removed from the mold, the spheres were melted on a flat aluminum plate until all that was left

was a disc 2.1 in (55mm) in diameter and 0.1 in (3mm) thick. The SHI was melted such that only clear ice was in the disc.

C. High Speed Camera SHI Production

Because the cotton-SHI specimens were completely white, it was difficult to obtain high speed video pictures with enough contrast to see crack development. Clear ice SHI samples were prepared as normal. For the cotton tests, 4g of cotton were used. In order to visually track the crack propagation during crush testing, the SHI was prepared with the addition of 3g of the dye Rhodamine B added to the water. After a single use, the dye stained the mold red. All subsequent SHI spheres had a slightly pink tinge which provided enough color contrast to see cracks develop in the high speed video footage.

D. Fracture Toughness and Compression Cube Specimen Production

In addition to spheres, testing also required column samples of SHI with a constant cross section. The overall process of preparing samples for testing was to use a rectangular mold to contain and freeze a known amount of cotton and water, cut the frozen samples to size, and then test the specimens. This process required several steps. An aluminum foil pan measuring $13\,{}^{1}/_{2} \times 9\,{}^{5}/_{8} \times 2\,{}^{3}/_{4}$ in (343 × 244 × 70 mm) was used as a mold for the samples. This was a satisfactory mold because it was cheap, flexible, and did not stick to the ice. To prevent spills, the foil pan was placed in a plastic tub. First, 4 liters of regular tap water was added to the mold. No attempt was made to purify or degas the water. To the water was added shredded cotton from cotton balls. The amount of cotton added varied according to the batch. To cover a range of concentrations, from clear ice to the ASTM F320 standard of 12% cotton by

mass, cotton was added to the mold in four different concentrations: no cotton, 130 g, 180 g, and 360 g of cotton. These amounts were estimated to correspond to 0%, 4%, 5.5%, and 10% cotton by mass, respectively, and each batch will be referred to as such throughout the section. It is important to note that the actual concentration differed for each specimen, but could only be accurately determined after testing had concluded as will be described later. Individual cotton balls were shredded by hand and randomly arranged in the water. Once shredded, this cotton-water mixture was then frozen overnight at -7°F (-22°C).

The frozen ice block was cut into individual test samples by hand on a band saw. Samples were trimmed from a block to prevent the edge effects that would occur from using an individual mold. Each block for use in fracture toughness tests was trimmed by hand on a band saw to measure 8.6 × 1.5 × 1.5 in (220 × 40 × 40 mm). Using these dimensions, each block could create seven test samples. Specimens for use in compression strength testing were trimmed to 1.5 × 1.5 × 1.5 in (40 × 40 × 40 mm). It was discovered that the samples cut best when pulled right out of the freezer with the saw running at the fastest available saw speed. Corrugated cardboard was used to prevent the block from coming into direct contact with the relatively warm steel saw table. Samples were refrozen as necessary throughout the cutting process and refrozen overnight before testing.

IV. Experiments and Results

A. SHI Disc Internal Crystal Photographs

Ice is made of individual crystals which form together. These crystals are invisible to the naked eye, but can be observed when viewed through two orthogonal, polarized lenses. This method was used to photograph the crystals within a SHI specimen. These photographs served two main purposes. The first was to determine the number and size of crystals within the SHI. If there are enough crystals within a sample, generally more than 10 across any linear dimension, the ice follows polycrystalline behavior and can be considered isotropic [24]. The second purpose was to determine how cracks spread across grains. Because the ice crystals within the SHI are at different orientations, the boundaries between each grain can be readily observed when seen through the lenses. The first sample, shown in Figure 15, has grains ranging in size from 3-30 mm. Also, there are apparently more than 10 crystals, meaning that the ice within the samples may be considered isotropic.

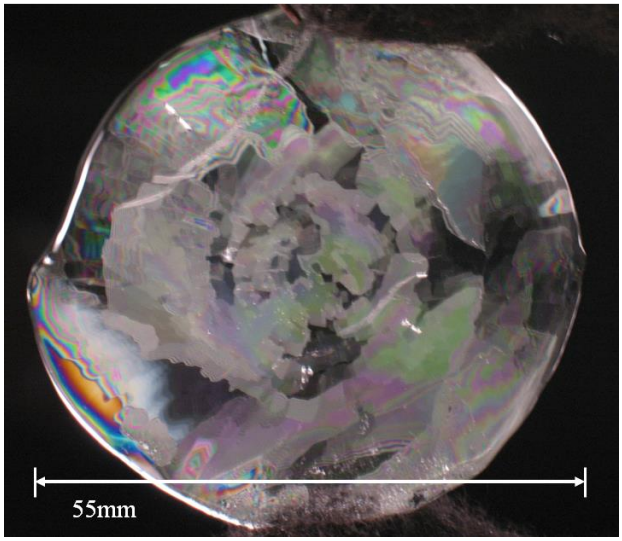

Figure 15: SHI Disc [0.1 in (3 mm) thick, 2.1 in (55 mm) diameter] Showing Crystal Structure

The second disc, shown in Figure 16, visibly cracked during preparation due to thermal shock. Though it is more difficult to identify individual grains in this sample than in the previous, it is readily apparent that cracks do not necessarily develop along grain boundaries. This means that future models of SHI do not need to be made up of individual crystals, but rather the SHI can be considered one isotropic material.

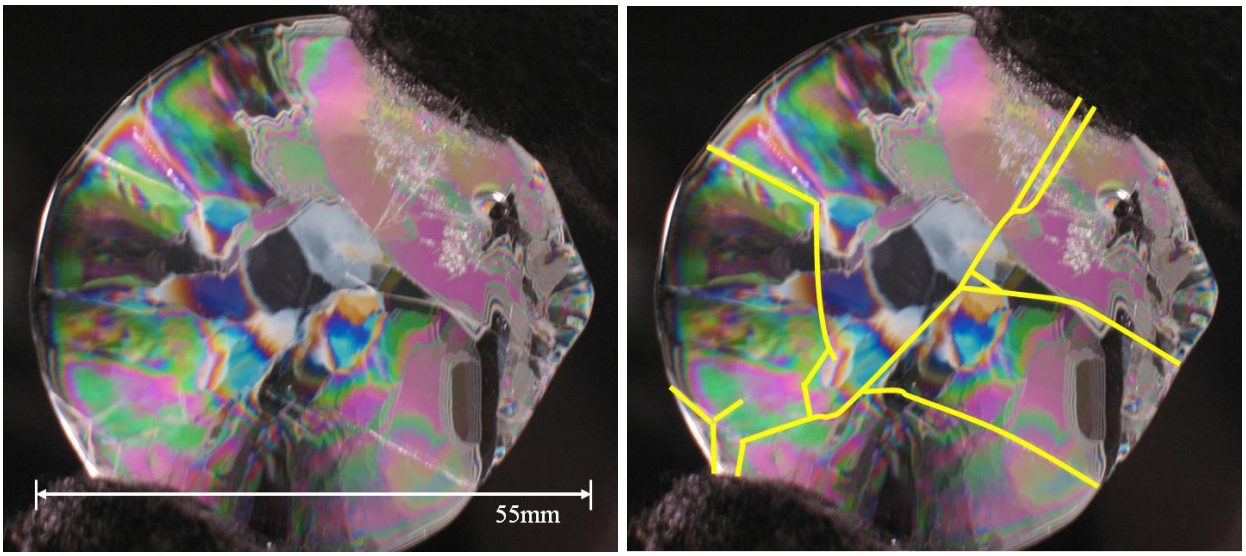

Figure 16: SHI Disc with Cracks Highlighted

B. Spherical Crush Tests

SHI samples were crushed at quasi-static strain rates to determine the load-displacement curves. The tests varied the size, strain rate, and cotton content of the SHI. Though initial tests varied the size, the decision was made to focus on testing the 2.5 in (63.5 mm) SHI. This was done because the larger spheres were easier to work with and yielded more consistent results. Results will only be reported for that diameter SHI.

1. Test Description and Procedure

Crush tests were conducted using SHI with different cotton concentration at various quasi-static strain rates. The machine used was an Instron 8801. A load cell with a maximum rating of 1124 lbf (5 kN) was used for the 0.5 in (12.7 mm) SHI tests; a load cell with a maximum rating of 22480 lbf (100 kN) was used for the other SHI diameters. The two machine heads each had an aluminum plate attached, providing a rigid contact surface. Because the machine was set up in a room temperature environment, each plate was cooled to 7°F (-22°C) before testing in the same freezer storing the SHI samples.

The machine head moves at a maximum crosshead displacement rate of 1 in/s (25.4 mm/s), establishing a limit on the strain rate tests. The definition of strain rate used was

$$\dot{\varepsilon} = \frac{V_{head}}{D} \tag{3}$$

where V_{head} is the crosshead displacement rate and D is the SHI diameter. The final test matrix used is shown in Table 3.

Table 3: Quasi-Static SHI Crush Test Matrix

SHI	Strain Rate (1/sec)						
	0.01	0.052	0.1	0.4	0.5	1.0	2.0
0.5 in (12.7 mm)/ clear	3	-	3	-	-	5	3
0.5 in (12.7 mm)/ cotton	-	-	-	-	-	4	-
1.0 in (25.4 mm)/ clear	2	-	2	-	3	4	-
1.0 in (25.4 mm)/ cotton	4	-	-	-	4	-	-
2.0 in (50.8 mm)/ clear	5	-	3	-	5		
2.0 in (50.8 mm)/ 4g	3	-	-	-	3		
2.0 in (50.8 mm)/ 8g	2	-	-	-	1		
2.5 in (63.5 mm)/ clear	5	5	2	5			
2.5 in (63.5 mm)/ 2g	5	2	-	6			
2.5 in (63.5 mm)/ 4g	5	-	-	10			
2.5 in (63.5 mm)/ 6g	5	2	-	7			
2.5 in (63.5 mm)/ 8g	4	-	-	6			
2.5 in (63.5 mm)/ 15.6g	4	-	-	5			
Total	47	9	10	39	16	13	3
Total Tests	137						

Crush test focus:
2.5 in (63.5mm) spheres

Note: The darkened region denotes the tests which exceed the machine's maximum crosshead displacement rate

The Instron machine can be controlled using both a manual interface and a software package. Before testing, limits were set to prevent damage to the machine or load cell. Each test was set up to automatically stop if the load reached 90% of the maximum load cell rating or if the machine head traveled half the diameter of the SHI, whichever came first. Data was gathered at 5 kHz at and above strain rates of 0.1 1/s and 1 kHz below strain rates of 0.1 1/s. The test procedure definition and data acquisition was done on a computer connected to the machine using the Instron provided software WaveMaker Editor and WaveMaker Runtime, respectively. The first program creates a file defining the test procedure, data collection, and data output. The second program then executes the file and records the data.

After setting up the test procedure software and machine, the SHI was removed from the freezer, weighed, and placed on the chilled aluminum plates. Pictures of the machine and setup

are shown in Figure 17. The distance between the plates was reduced until the SHI almost touched the top plate at which point the test was run. Afterwards, the fractured SHI was removed, the data was recorded, and the test procedure software and machine were reset for the next test. In between tests, cold packs were placed on the aluminum plates to keep them cold. Because the SHI were temperature sensitive, the tests were always completed within 30 seconds of removing the SHI from the freezer. It was also discovered that the aluminum contact plates needed to be removed from the Instron and refrozen after every four tests.

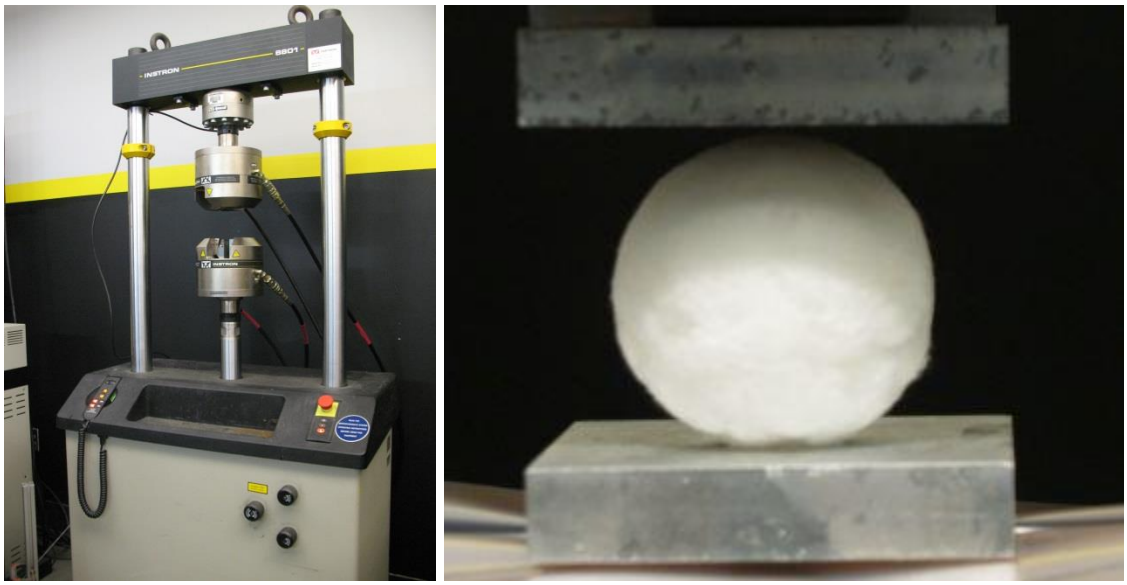

Figure 17: Instron 8801 Machine (L) with SHI Test Setup (R)

As testing progressed, the decision was made to focus on the 2.5 in (63.5 mm) SHI at two different strain rates. It was discovered that the larger SHI spheres were the easiest to consistently manufacture and test. It was relatively easy to vary the percentage of cotton from 0% (clear) to 12% (ASTM F320 standard), which is equivalent to 15.6 g of cotton for the 2.5 in (63.5 mm) SHI. The 2.5 in (63.5 mm) SHI did not melt quickly, and the results showed less

scatter when compared to the smaller SHI diameters. It also generated high enough loads under compression to reduce the relative effect of the load cell signal noise.

To determine the effect the warm room testing environment has on the specimens, a FLIR SC620 Infrared Camera was used to measure the temperature of the specimens before testing. Even though the SHI was stored at -7°F (-22°C), it would begin to warm as soon as it was removed from the freezer. Keeping the aluminum plates stored in the freezer helped reduce melting. At testing, as can be seen in Figure 18, the SHI temperature was 7°F (-14°C).

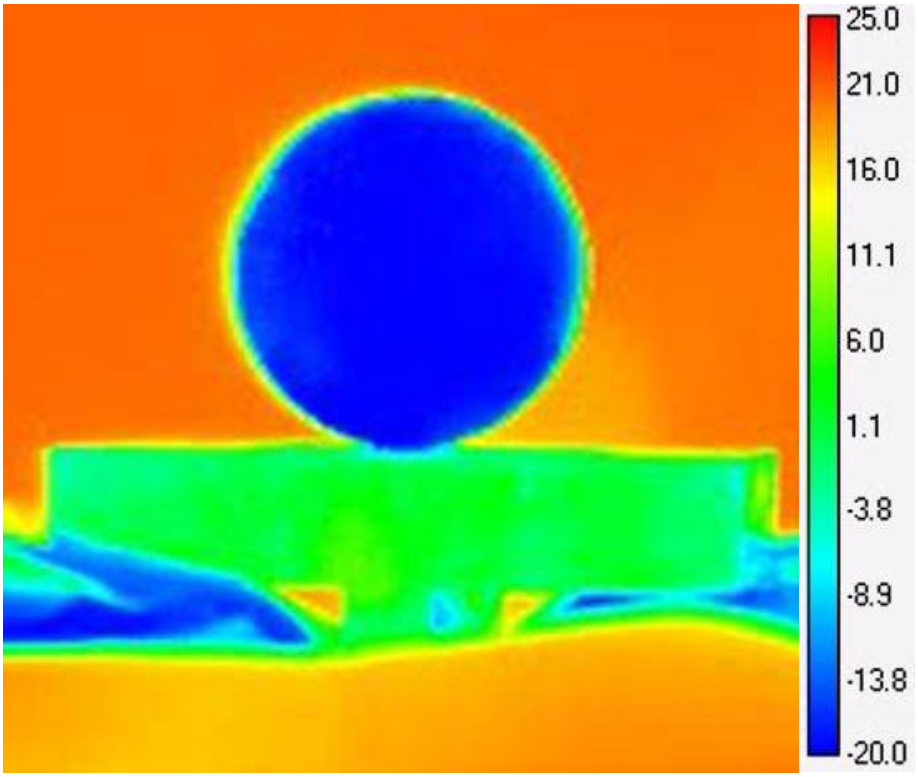

Figure 18: SHI Thermal Picture, Pre Fracture [36]

2. Test Results

Because SHI testing was done using spheres as opposed to cylinders of constant cross section, it is not directly possible to measure the SHI strength or stiffness. The load-displacement curves from the crush tests are only directly comparable to other spherical objects.

Every type of 2.5 in (63.5mm) SHI was tested at two displacement rates: 0.01 and 0.4 1/s, hereafter referred to as the "slow" and "fast" strain rates, respectively. The raw force-displacement test data is shown in Appendix A and B. The crush data is represented by average linear curves for each amount of cotton, as shown in Figure 19 and Figure 20, for the slow (0.01 1/s) and fast (0.4 1/s) strain rates, respectively. These linear curves reveal the overall trends in the data.

For both strain rates, the clear and cotton-SHI failed in different manners. At the slower strain rate, the clear-SHI behaves in a brittle manner. At failure, the SHI cleanly breaks into distinct shards and does not carry any additional load. However, the cotton-SHI behaves in a ductile manner. The load increases until some critical load at which point the SHI continues to carry a load but at a reduced stiffness. Increasing the amount of cotton in the SHI increases the amount of energy necessary to separate the cotton fibers from the ice after initial failure. Unlike the clear-SHI which breaks into several individual pieces, the cotton-SHI flattens into a disc.

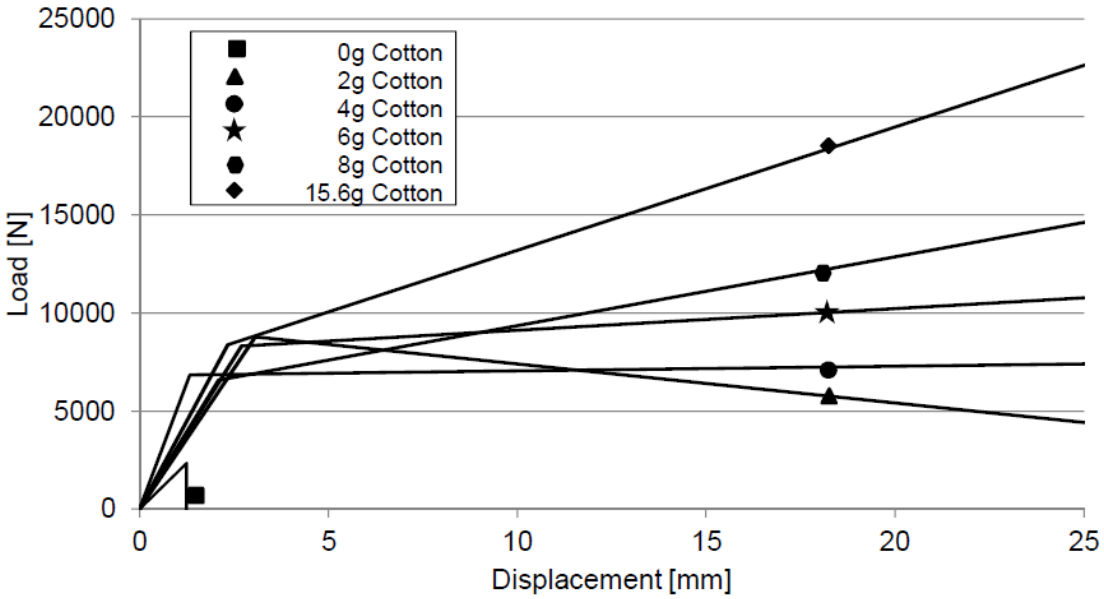

Figure 19: Simplified Data Curves, 2.5 in (63.5 mm) SHI, Strain Rate = 0.01 1/s [36]

At the higher strain rate, 0.4 1/s, the clear-SHI exhibits the same brittle tendencies while the cotton-SHI undergoes three loading phases, as shown in Figure 20. In the first phase, the SHI carries the load until an initial critical load is reached. After that the stiffness decreases but the SHI continues to carry an increasing load until a second critial load (maximum load). Past the maximum load, the SHI carries decreasing force as the cotton fibers continue to separate from the SHI. Unlike the slow speed tests, the cotton-SHI breaks into several distinct pieces similar to the clear-SHI.

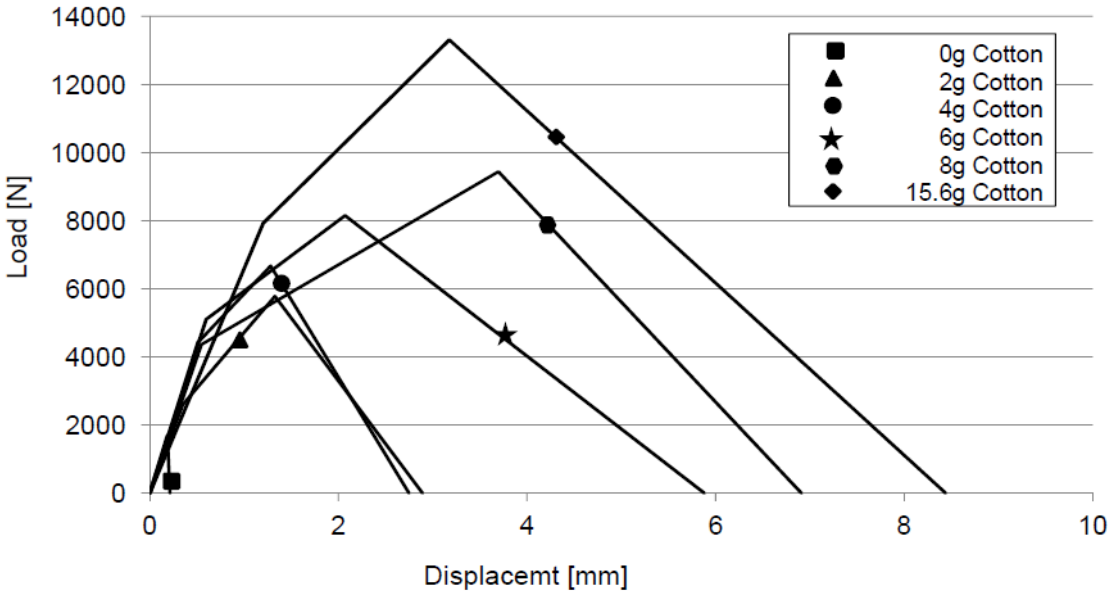

Figure 20: Simplified Data Curves, 2.5 in (63.5 mm) SHI, Strain Rate = 0.4 1/s [36]

Adding cotton to the SHI increases the amount of work it takes before failure, as shown in Figure 21 and Figure 22. Work is defined as the area under the load-displacement curve. For all cotton amounts, increasing the strain rate decreases the work to failure. This is due to the combined effects of creep and fiber crack bridging. Increasing the strain rate decreases the amount of time the SHI has to deform.

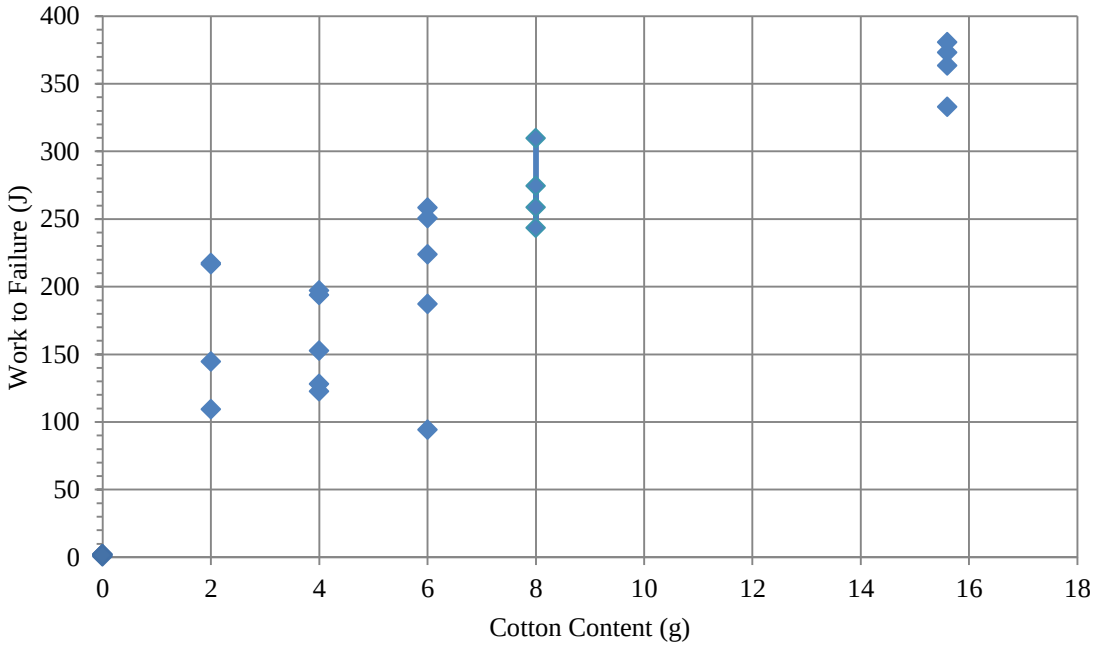

Figure 21: Work to Failure, 2.5 in (63.5 mm) SHI, Strain Rate = 0.01 1/s

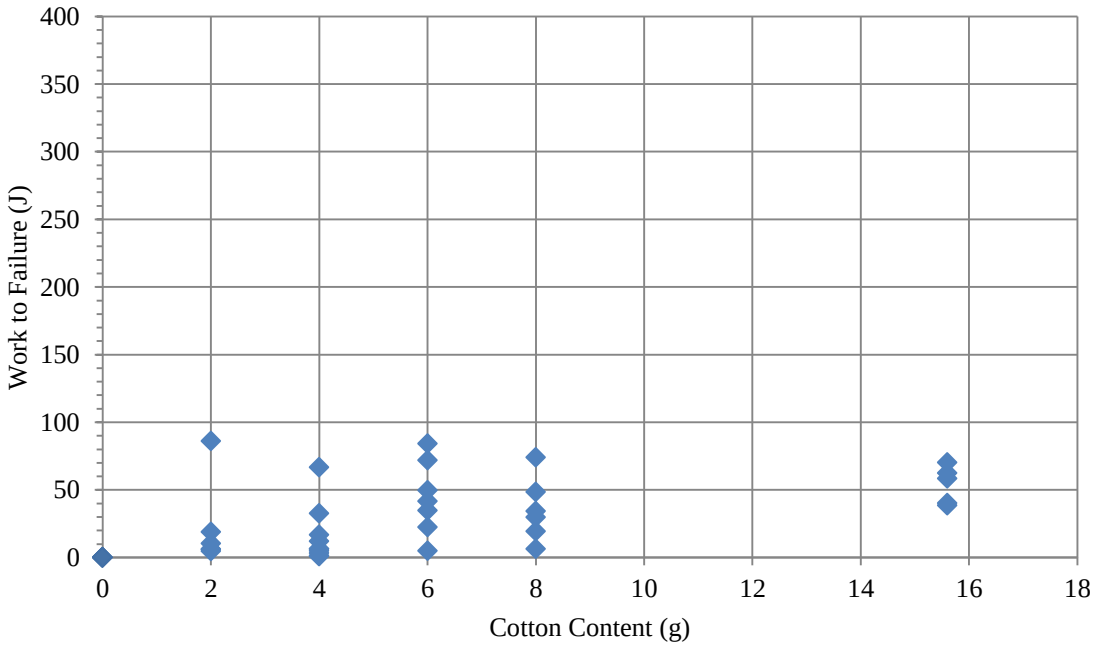

Figure 22: Work to Failure, 2.5 in (63.5 mm) SHI, Strain Rate = 0.4 1/s

3. Initial Data Analysis

Though the stresses in the spherical SHI cannot be directly measured from the data, it is possible to estimate the tensile and compressive strength of ice using analytical solutions developed by Hiramatsu and Oka for tensile strength [30] and Russell and Wood for compressive strength [35].

For clear ice, the estimated compression strength results of the SHI was overlayed with a chart compiled by Kim and Keune [20], as shown in Figure 23. The chart shows an increase in compression strength as the strain rate increases, but does not line up well with the results from dedicated compression tests. The most important conclusion to draw from the results is that the equations only give an estimated compression strength for a perfectly brittle material. Ice is not a perfectly brittle material, even at higher strain rates.

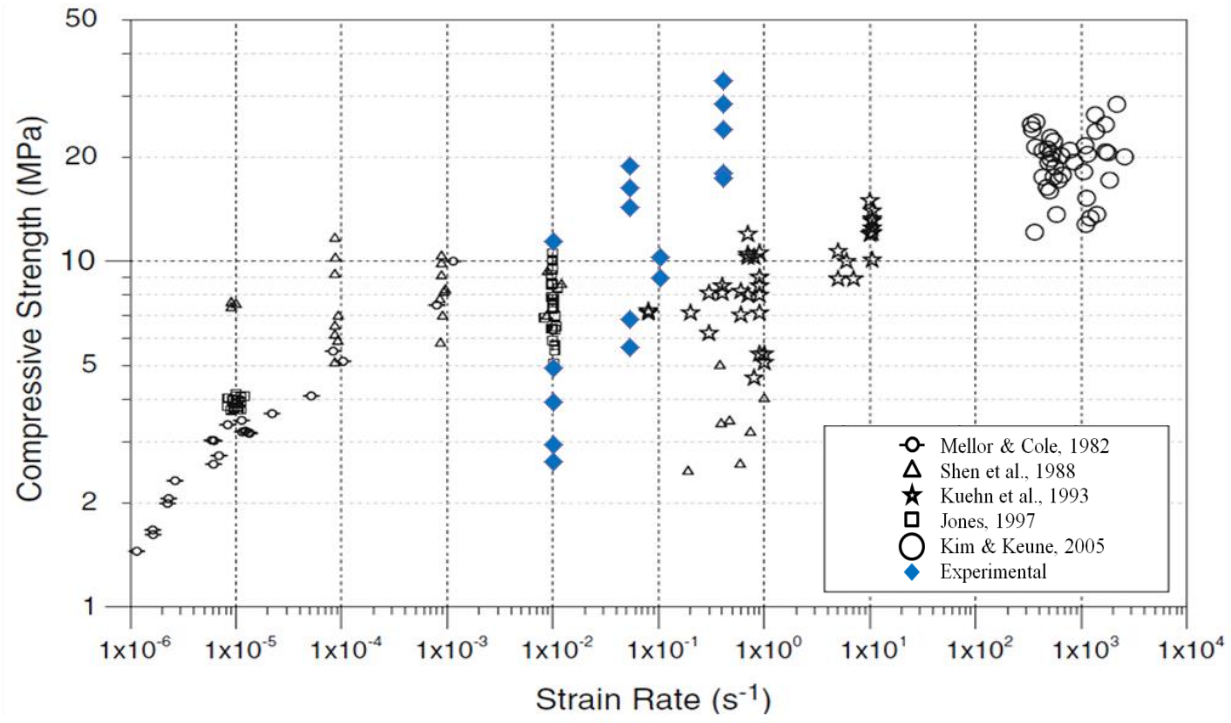

Figure 23: Estimated Compression Strength, 2.5 in (63.5 mm) SHI, Clear Ice

According to Schulson [20], the tensile strength of ice varies between 0.5 and 1.5 MPa, with an average of about 1.0 MPa. As previously mentioned, a good rule of thumb to use is that the tensile strength of ice is an order of magnitude less than the compression strength. Unlike compression strength, tensile strength stays relatively constant over a wide range of strain rates. The estimated tensile strengths from the tests, as a function of strain rate, are shown in Figure 24, along with the tensile strength range reported by Schulson. As with compression, the perfectly brittle material assumptions used to develop the tensile strength equations are not perfectly valid, tending to underestimate the results.

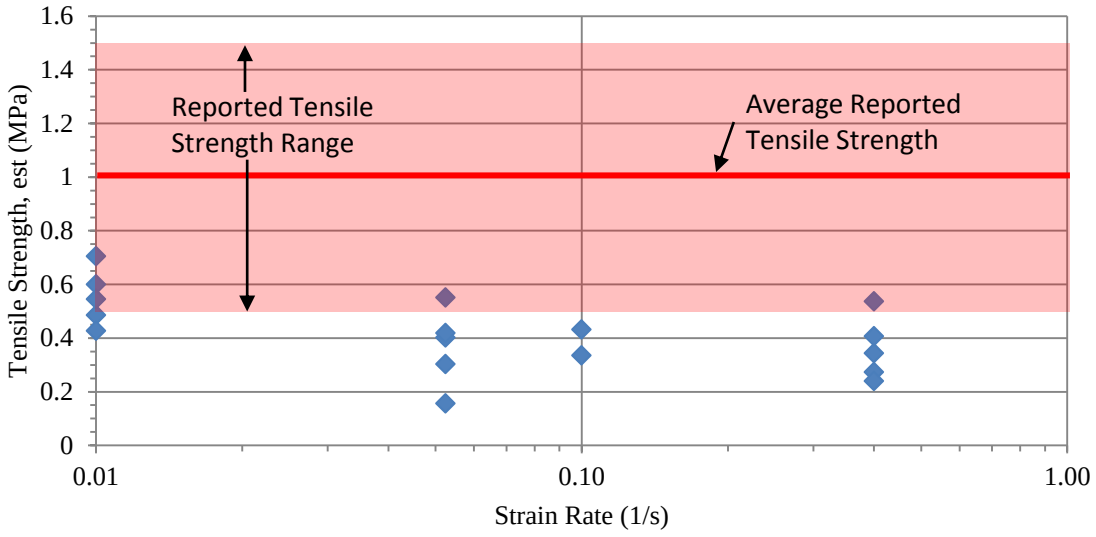

Figure 24: Estimated Tensile Strength, 2.5 in (63.5 mm) SHI, Clear Ice

Applying compression and tensile strength estimate equations (Eq. 1,2) to the cotton filled SHI at the fast strain rate results in the tensile estimates as shown in Figure 25 and the compression estimates as shown in Figure 26. As can be seen in the tensile estimate, adding cotton significantly increases the strength of the SHI. The strength increases from an average of 0.36 MPa with clear ice to 3.17 MPa with 15.6g cotton, an increase of 781%.

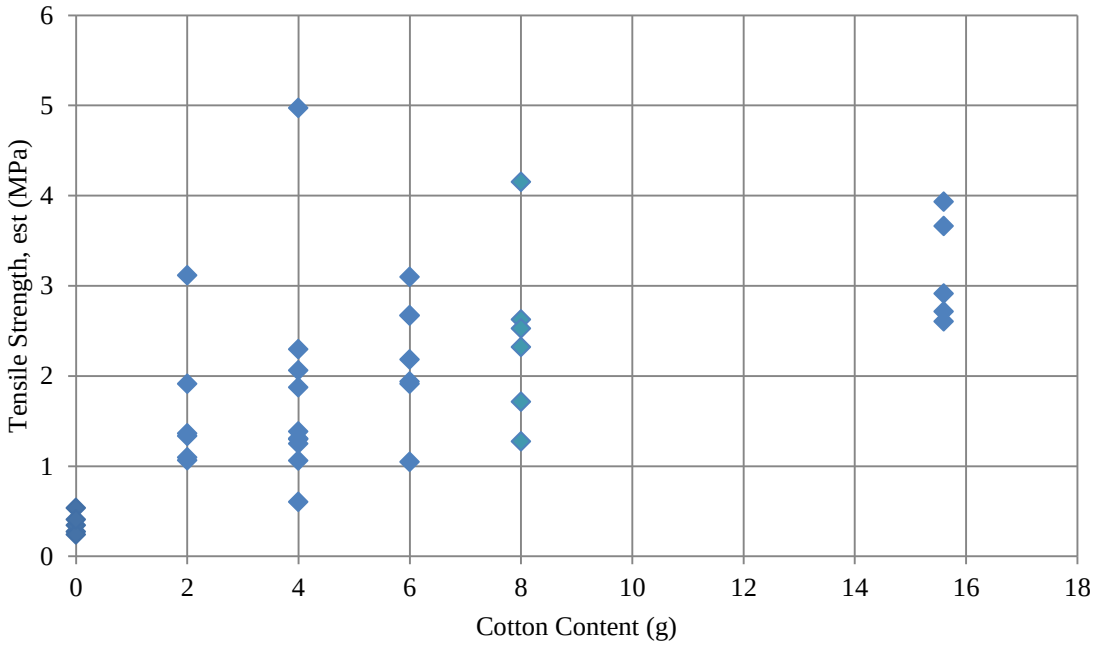

Figure 25: Est Tensile Strength, 2.5 in (63.5 mm) SHI, Strain Rate = 0.4 1/s

Unlike the tensile estimates, the compression strength estimate does not greatly increase with increasing amounts of cotton. The average compression strength at 0g cotton is 24.29 MPa which increases to 26.41 MPa at 15.6g cotton, an increase of 49%.

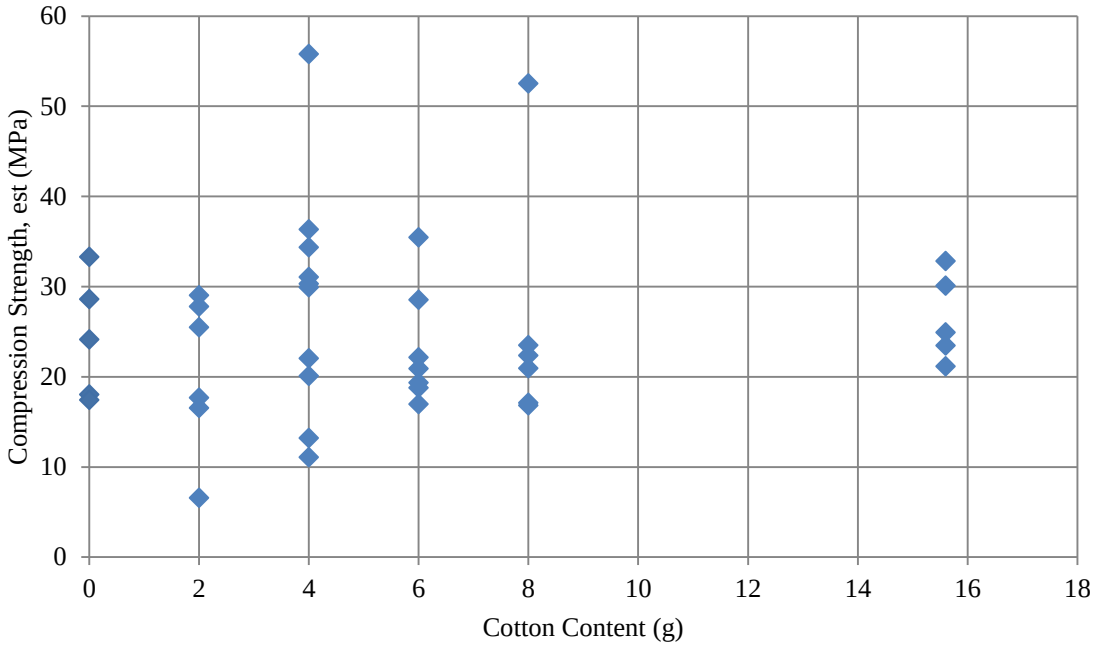

Figure 26: Est Compression Strength, 2.5 in (63.5 mm) SHI, Strain Rate = 0.4 1/s

The compression strength data of the SHI will be tested in a second manner and further conclusions will be drawn in a later portion of this report.

4. Conclusions

The crush test results of the SHI show that the amount of cotton filler and the quasi-static test strain rate have a tremendous impact on how SHI fails. At all of the tested strain rates, the clear-SHI behaved in a brittle manner. The load increased until some failure at which the SHI cleanly broke into multiple pieces. However, the cotton filled SHI failed in a ductile manner. At the slow strain rate the SHI crushed into a disc without breaking into multiple pieces. This is due to the additional energy needed to separate the cotton fibers. Increasing the strain rate was shown to decrease the amount of energy necessary for failure. The faster the strain rate, the smaller the effect which material creep has on the overall behavior.

An attempt was also made to estimate the strength of the ice using equations from Hiramatsu and Oka for tension and Russell and Wood for compression to compare with clear ice strength values. In both cases the estimates varied significantly from established literature values. This is not surprising considering the difference in the material behavior of SHI and perfectly brittle materials for which the equations were developed. The equations should not be used to directly compare spherical SHI results with established literature data. However, the equations are useful in identifying trends within the data.

C. High Speed Photography

A high speed camera was used to document the failure methods and crack propagation in spherical SHI during crush testing. The goal was to use a camera to document the failure mode as well as help interpret quasi-static crush test data. High speed footage was taken of both clear and 4g cotton-SHI. Because the presence of cotton significantly changes the SHI force-displacement curves, it was appropriate to obtain footage for both conditions.

1. Test Description and Procedure

Test samples were prepared as mentioned in the sample manufacturing section. A Vision Research Phantom 12.1, one million frame-per-second high speed camera was used to obtain high speed camera footage. High speed footage was shot during crush testing at 25000 pictures per second (pps), 512x384 resolution, with the exposure rate at 39.559 μs. The camera contains 8 GB of internal memory. Using these settings, the camera could record 28528 frames, or approximately 1.14 s, of footage. The lens was manually focused on the front surface of the SHI. The camera was controlled using the manufacturer provided Phantom Camera Control (PCC) software connected to a laboratory laptop specifically networked to interface with the camera. To provide light for the camera, four spotlights were placed around the test machine. The machine setup was identical to other SHI crust tests

After setting up the camera, the final step was to prepare the SHI for testing. When stored in a plastic bag kept in a freezer, clear-SHI tends to develop ice crystals on the surface, creating a frosty layer which prevents the camera from clearly documenting crack development. To remove the surface crystals without melting the SHI, immediately prior to testing each sample was lightly rubbed by hand while wearing woolen winter gloves until the surface was

clear. A single drop of water from a damp paper towel placed on the surface of the sample helped speed the process. The cotton-SHI was not rubbed in this manner as it did not improve the visibility of seeing the cotton. The SHI was then placed in the machine, the spotlights were turned on, and the SHI was tested within 1 min of being removed from the freezer. About half of that time was used to remove the surface crystals with the remainder being the time necessary to place the sample in the machine.

With the addition of the high speed camera setup, the test procedure was identical to the SHI crush tests. The Instron was set to run at the displacement rate of 1 in/s, which corresponds to the SHI strain rate of 0.4 1/s. Data was recorded at 5 kHz. It took six attempts for the clear and three attempts for the cotton-SHI to obtain quality high speed video.

2. Data Reduction and Analysis

Due to differences in the testing condition, the load-displacement data cannot be directly compared to other clear or cotton-SHI tests. Recall that in these tests, the clear-SHI surface was warmed to show clear ice throughout the sphere. The aluminum contact plates also warmed quickly under the hot spotlights, resulting in some melting along the bottom contact surface. These all significantly increased the SHI temperature.

Using the PCC software, the footage was analyzed and compared to the force-displacement curve from the Instron. The two were correlated by synchronizing the moment of contact in both the data and the footage. The raw machine data was post processed using Microsoft Excel. The clear and cotton ice load-displacement data results are shown in Figure 27 and Figure 28 respectively, each with accompanying stills from the footage.

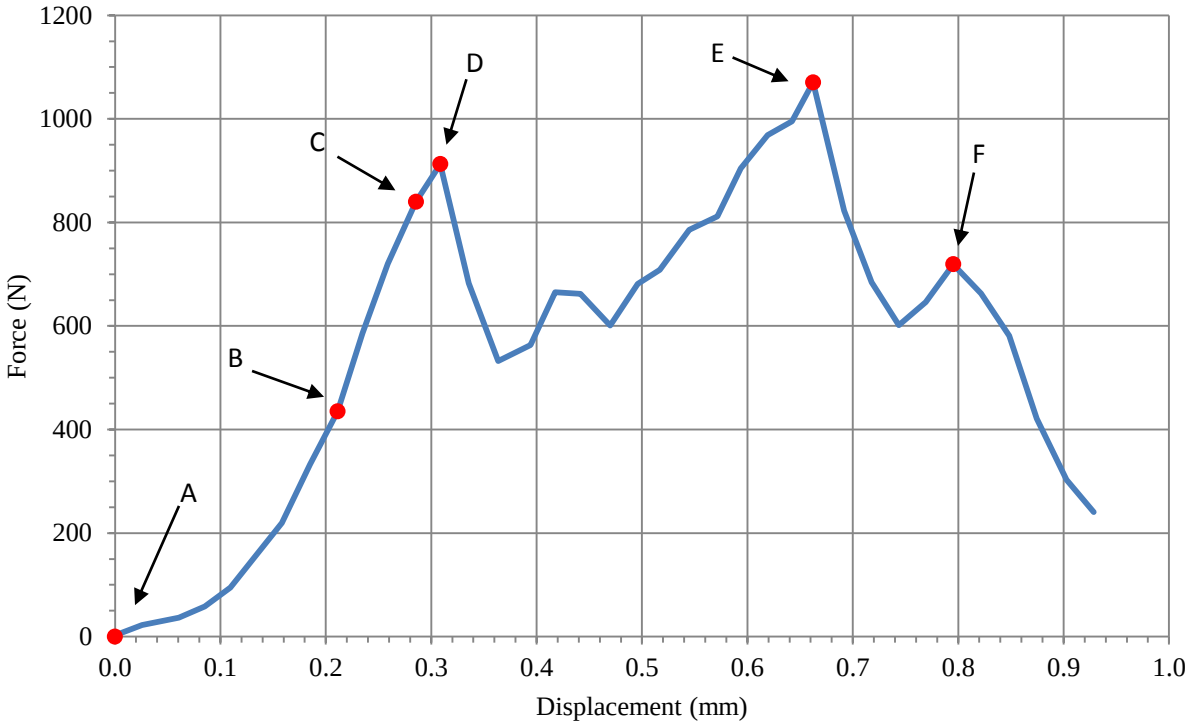

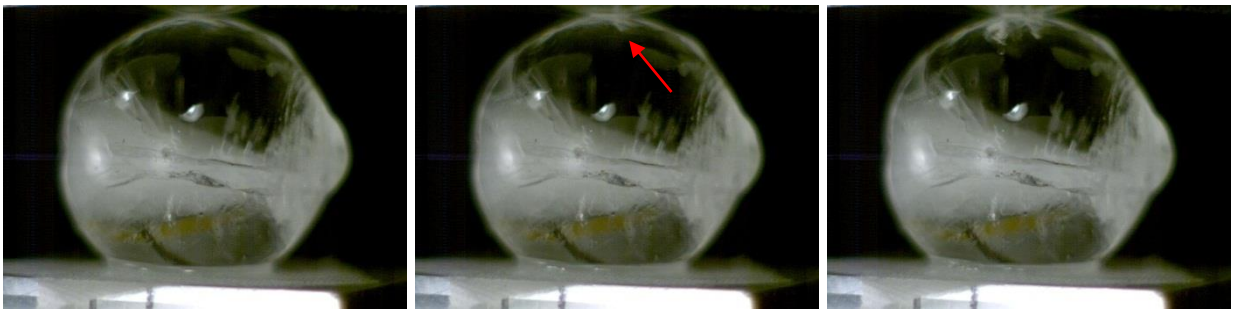

A) Moment of contact
$t = 0\ sec$

B) Visible cracks appear
$t = 0.00876\ sec$

C) Onset of rapid crack propagation
$t = 0.01116\ sec$

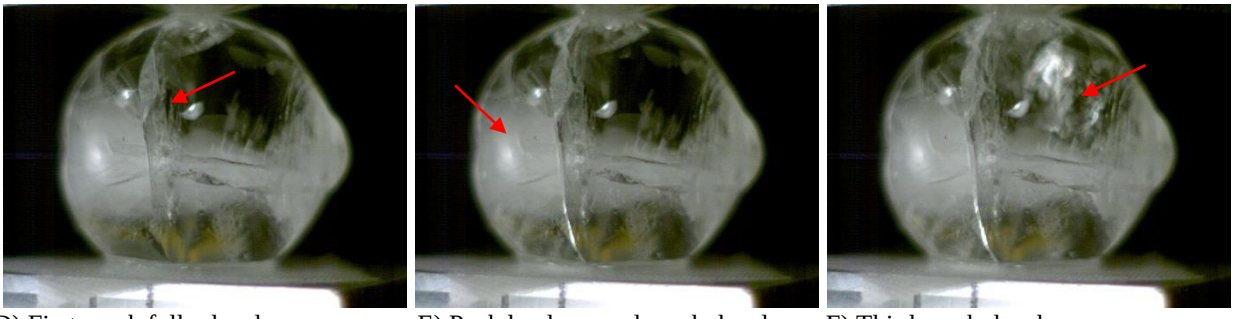

D) First crack fully develops
$t = 0.01248\ sec$

E) Peak load, second crack develops
$t = 0.02560\ sec$

F) Third crack develops
$t = 0.03108\ sec$

Figure 27: 2.5 in (63.5mm), Clear-SHI Quasi-static (Strain Rate = 0.4 1/s) Force-Displacement Curve with Corresponding High Speed Camera Photos

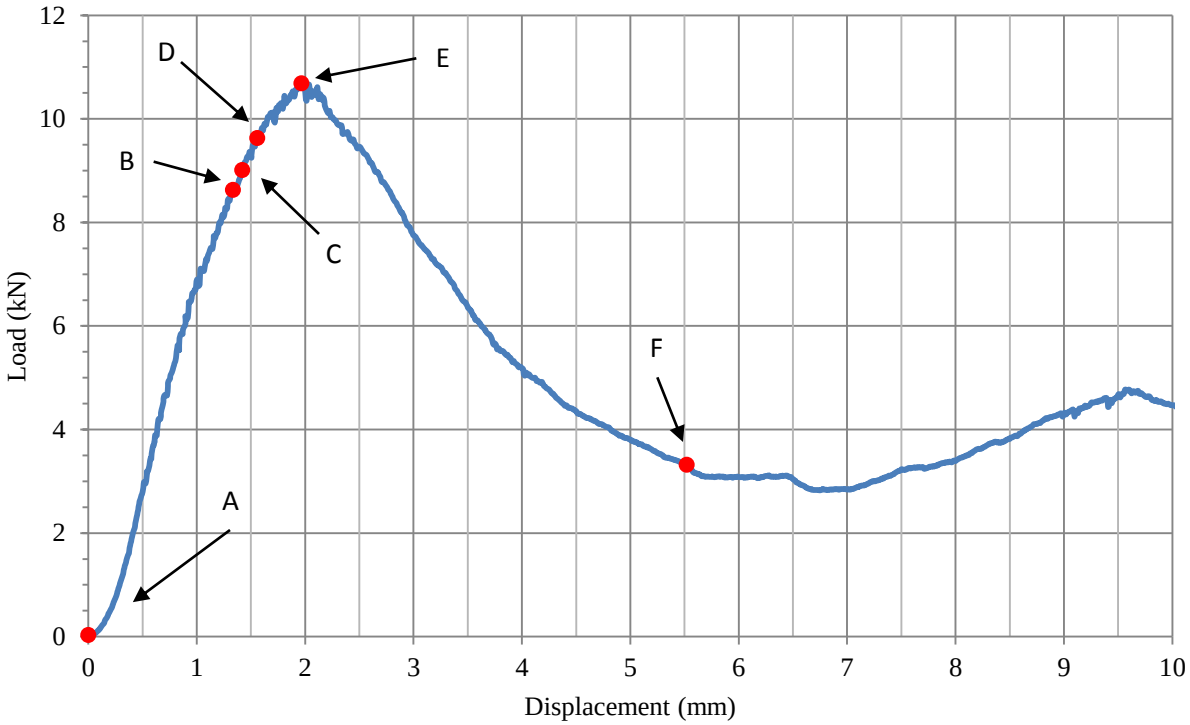

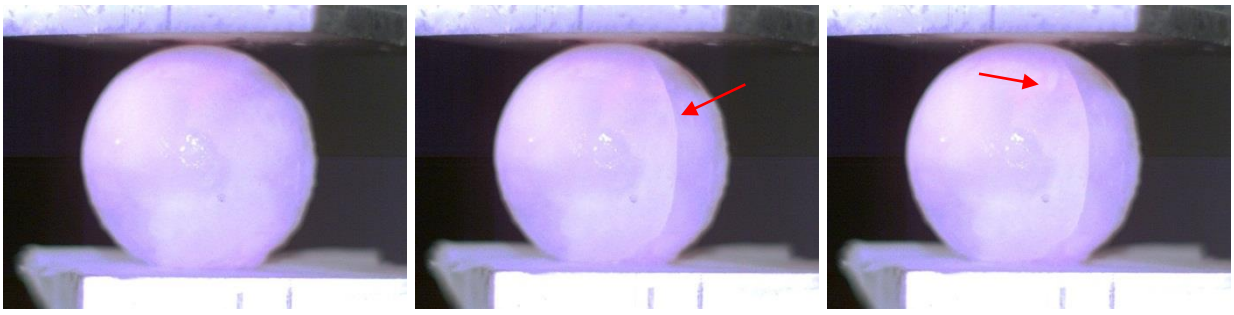

A) Moment of contact
$t = 0\ sec$

B) First visible crack develops
$t = 0.0528\ sec$

C) Second visible crack develops
$t = 0.0561\ sec$

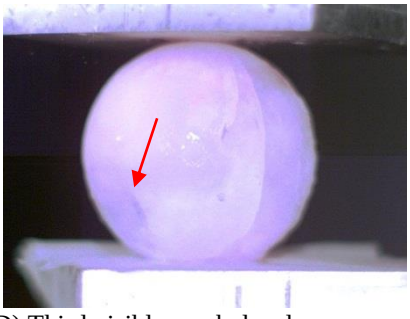

D) Third visible crack develops
$t = 0.0617\ sec$

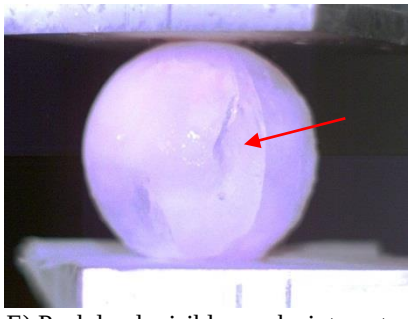

E) Peak load, visible cracks interact
$t = 0.0770\ sec$

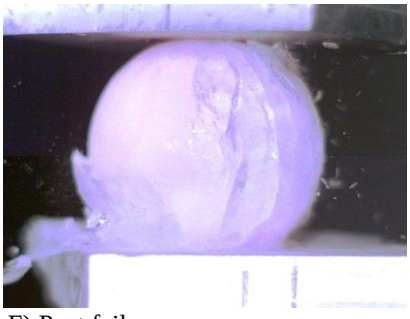

F) Post failure
$t = 0.2162\ sec$

Figure 28: 2.5 in (63.5mm), 4g Cotton-SHI Quasi-static (Strain Rate = 0.4 1/s) Force-Displacement Curve with Corresponding High Speed Camera Photos

As seen in the clear ice pictures, there was an initial crack at point D, Figure 27, but the footage shows that it did not split the SHI into two distinct pieces at this point. The SHI instead broke into two distinct pieces at the point of maximum load, point E. Additional peaks, such as at point F, correspond to the creation of more cracks. The clear ice failed when one or two major cracks developed and interacted, causing an overall failure.

For the cotton ice tests, failure occurred after several smaller cracks began to interact. This can be seen both in the footage and in the data where there are many small peaks (points B-D, Figure 28), suggesting the formation of small cracks, before reaching the maximum load at point E when these cracks began to interact. After this point, the ice in the sphere has failed, but there is still cotton holding the broken ice together. There is additional energy necessary to separate the cotton from the ice, causing complete failure. This can lead to the sphere splitting into several distinct pieces as generally happened at higher strain rates or can lead to the sphere flattening into a disc as generally happened at the slower strain rates.

3. Conclusions

There are a number of important conclusions which can be drawn from these high speed camera tests. In particular, it was important to identify on the data curve when visible cracks appeared and, conversely, to identify in the video when peaks in the data occurred. That correlation is shown in the above charts and pictures.

The data shows that load peaks occur when cracks form. In both SHI cases, the peak load occurred when smaller cracks interacted to cause the overall failure of the SHI. As can be easily seen in the clear ice footage, cracks begin to form near the point of contact. As the sphere is compressed, the initial cracks grow slowly until some critical point when the crack growth becomes unstable. This suggests that the sphere is failing through a combination of compression

failure near the point of impact and tensile fracture failure through the center. As expected, crack formation correlates with a sudden decrease in the applied load, marked by the sharp peaks in the data curve.

In both cases, the SHI failed through a combination of compression failure and tensile fracture. Cracks initially form near the point of contact where the ice is in a state of compression. Eventually the cracks spread to the point where the sphere is under tensile stress. At that point, the cracks in the ice begin to spread catastrophically, limited only by the Mode I fracture toughness of the material. Thus, the video footage suggests that the clear and cotton-SHI fails through a combination of compression failure followed by tensile crack fracture. These two topics will be the focus of the testing for remainder of this paper.

D. Fracture Toughness

Literature review and high speed video research has indicated that SHI fails through a combination of compression and tensile fracture strength failure. Literature research has also indicated that while there have been numerous studies identifying the fracture toughness of clear ice, there has not been any significant research in determining the fracture toughness of cotton fiber reinforced ice, thus making the topic a significant area of research. Fracture toughness refers to a material's ability to resist crack formation and propagation. Of particular interest is Mode I fracture toughness, which resists the formation of cracks due to peeling stresses.

1. Test Description and Procedure

The Mode I fracture toughness, K_{IC} was obtained using a three-point bend test. Previous literature reviews had indicated that this was one of several viable methods used for testing K_{IC} [26]. Before testing, a notch was added to each sample using a band saw. The notch varied slightly for each sample, measuring from 1-2 cm in depth. A notched beam specimen and test setup is shown in Figure 29.

Figure 29: Fracture Toughness Beam Specimen and Test Setup

An Instron 8801 machine was used to test the samples. The load cell used was rated for 1124 lbf (5 kN). As noted previously, two manufacturer provided software programs, WaveMaker Editor and WaveMaker Runtime, were used to run the test program and collect the data. Attached to the load cell was a three-point bend jig capable of holding the test specimen. A piece of masking tape covering the roller points in contact with the specimens helped prevent the ice from moving or slipping in the jig. Styrofoam caps, measuring $1.5 \times 1.5 \times 0.25$ in ($40 \times 40 \times 7$ mm), were placed in between the rig contact points and the specimen. This was necessary to help control the specimen temperature.

After setting up the fixture, each specimen was measured and weighed. The notch, which was previously cut on a band saw, was scored using a fresh razor blade. The specimen was then placed in the fixture, the test was run, and the data was recorded. In all cases, the test stopped after the Instron had displaced 1.1 in (30 mm).

Because the exact cotton concentration was not known before testing, the specimens were weighed before testing. After testing, each used specimen was dried in an oven at 220°F (104°C) for 1-2 hours and the leftover cotton was also weighed. Comparing the dried cotton with the original mass gives the cotton concentration for that particular specimen.

A thermal picture of a specimen during testing is shown in Figure 30. The temperature at the center of the beam was 12°F (-11°C) at the moment of impact. There was some warming along the edges.

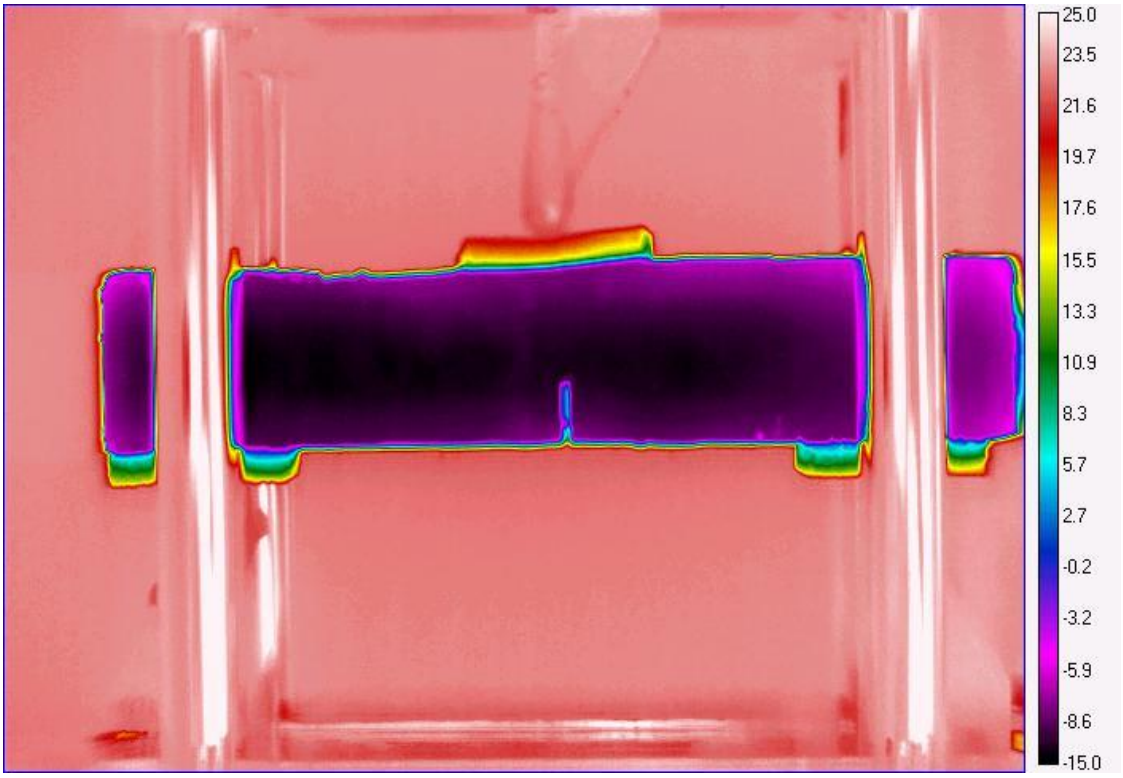

Figure 30: Notched Beam Thermal Picture, Pre-Fracture

2. Data Reduction and Analysis

The following equations from Murakami [37] were used to calculate the fracture toughness:

$$K_I = \frac{3SP}{2tw^2}\sqrt{\pi a}\cdot F(\alpha) \quad \text{where} \quad \alpha = \frac{a}{w} \quad \text{and} \quad F(\alpha) = \frac{1.99-\alpha(1-\alpha)(2.15-3.93\alpha+2.7\alpha^2)}{(1+2\alpha)(1-\alpha)^{3/2}} \tag{4}$$

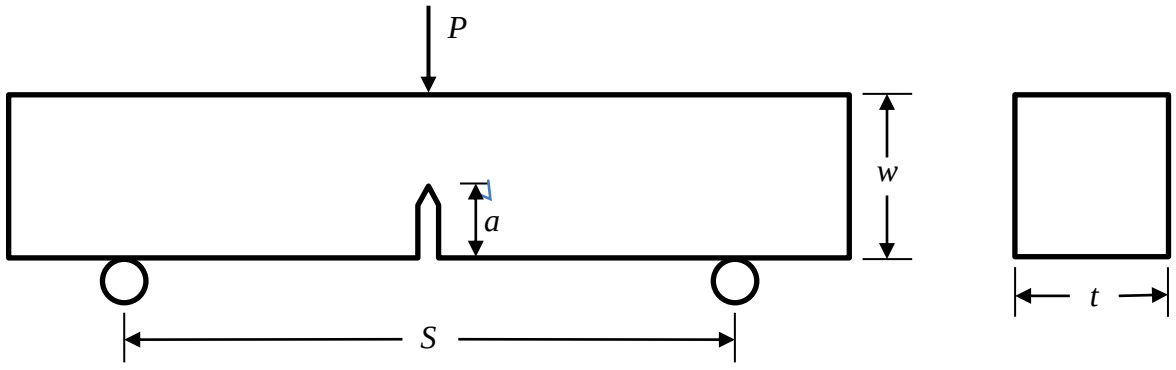

Figure 31: Three Point Bend Test Geometry

The first step in post processing the data was to determine if K_I was rate dependent. Previous research had indicated that at extremely low load rates, ice behaves in a ductile manner. This causes the notch to deform without breaking, resulting in a relatively high apparent fracture load. The fracture load decreases as the load rate is increased until the load rate reaches some critical rate, at which point any further increase in the load rate does not change the fracture load. This critical load rate represents the point at which the load is added to the ice so quickly that it does not have time to deform before breaking. This trend is shown in the data reproduced from Nixon and Schulson [26], overlaid with experimental data as seen in Figure 32.

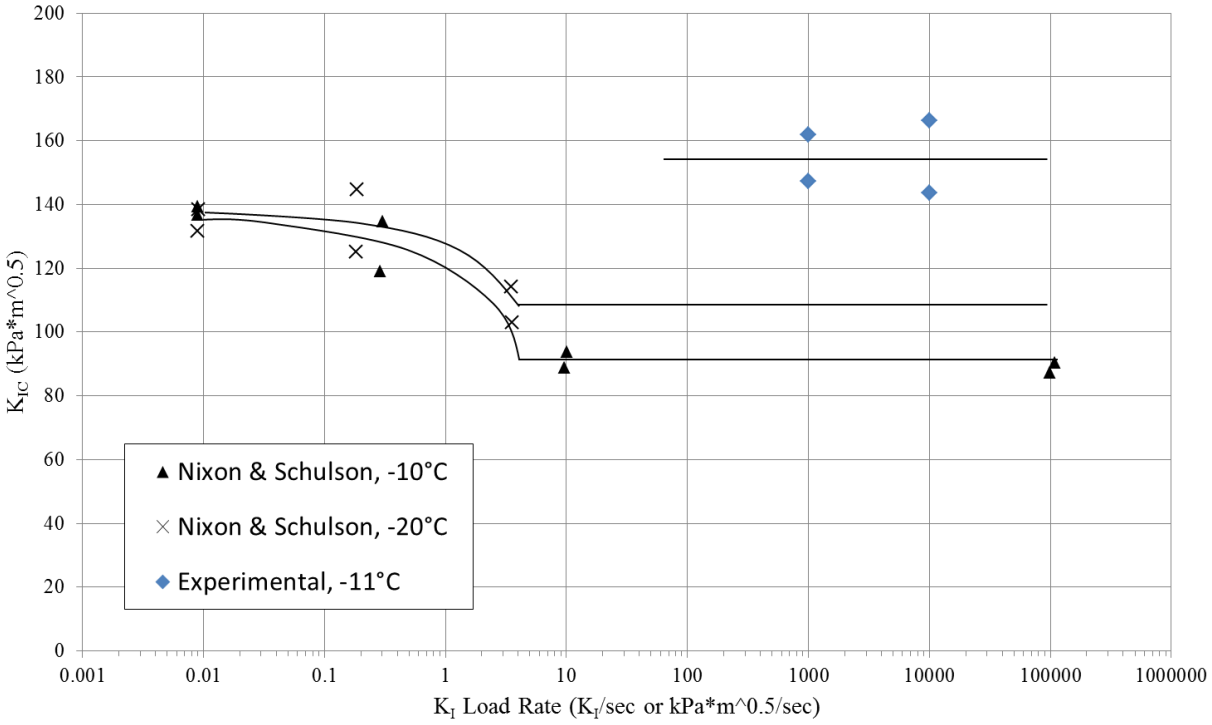

Figure 32: Clear Ice K_{IC} Rate Dependence, Experimental and Literature Data

As can be seen in Figure 32, the experimental data trends agree with the literature data. A significant difference between the literature test setup and this setup was in temperature

control. Adding styrofoam pads to the rig's three contact points greatly decreased the effect the room's temperature had on the results.

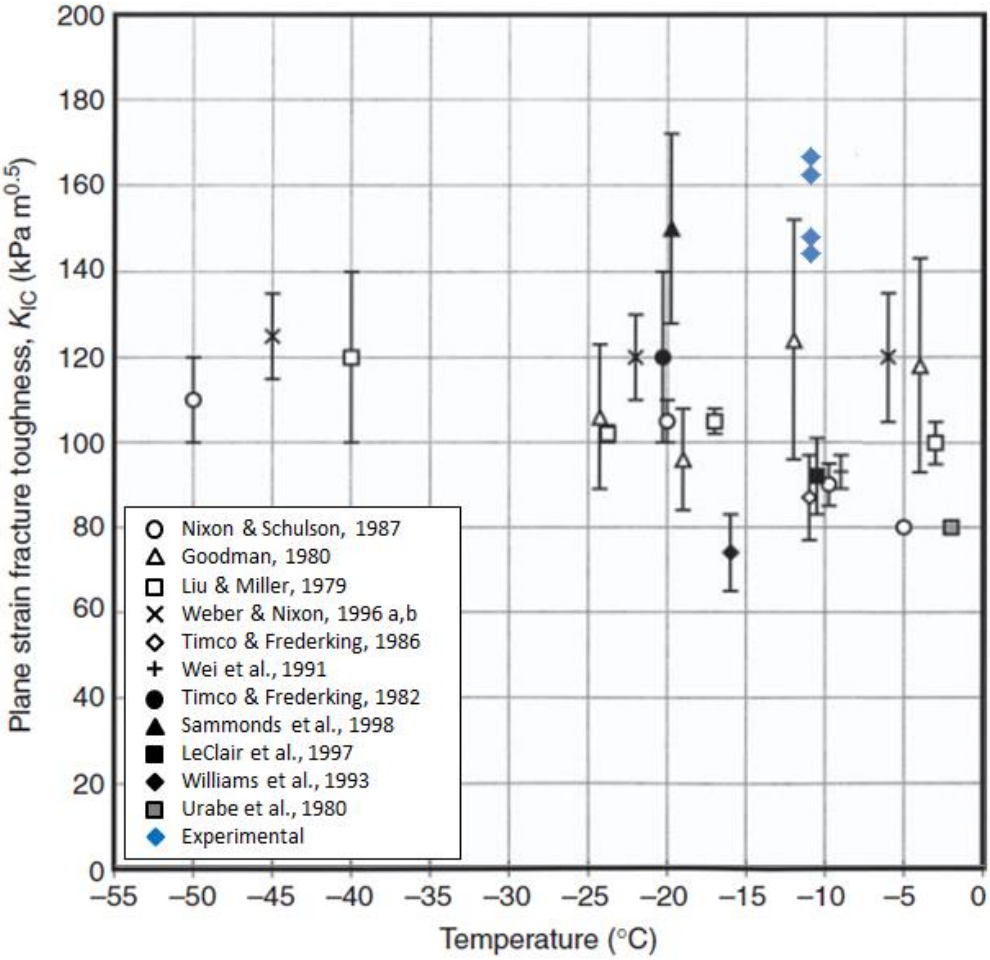

Figure 33: K_{IC} Literature Comparison

Having measured accurate data for the clear ice samples, the next step was to characterize the cotton reinforced ice, and investigate if it showed similar trends. The combined K_{IC} results for each of the four batches are shown in Figure 34.

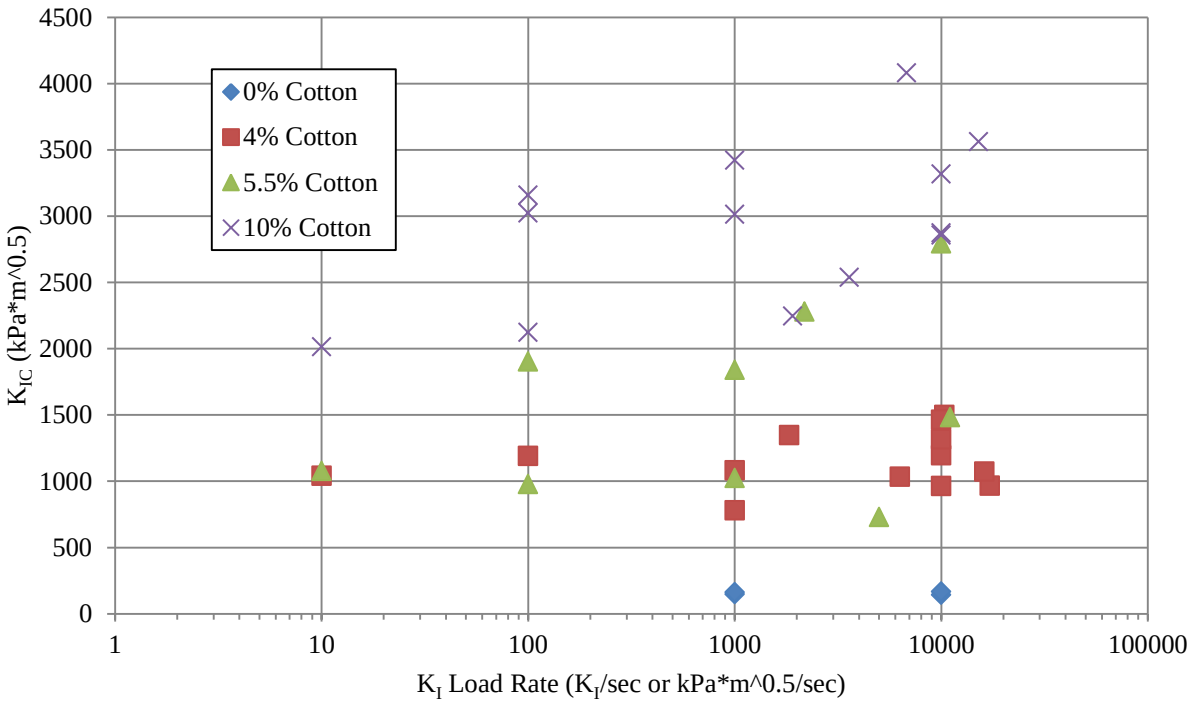

Figure 34: K_{IC} Rate Dependence

It was not possible to perform tests at a slower load rate than 10 K_I/sec because the loads were within the noise of the load cell. It was also not possible to exceed about 100000 K_I/sec, which corresponded with the crosshead displacement rate limit of the machine. It is difficult to draw specific conclusions from this data alone. Unlike the clear ice data in Figure 33, there does not seem to be any rate dependence for the cotton reinforced ice.

Once it was determined which data points could be used in drawing conclusions about the K_{IC} relationship, each data point was then correlated with its cotton concentration, the results of which are shown in Figure 35 through Figure 37.

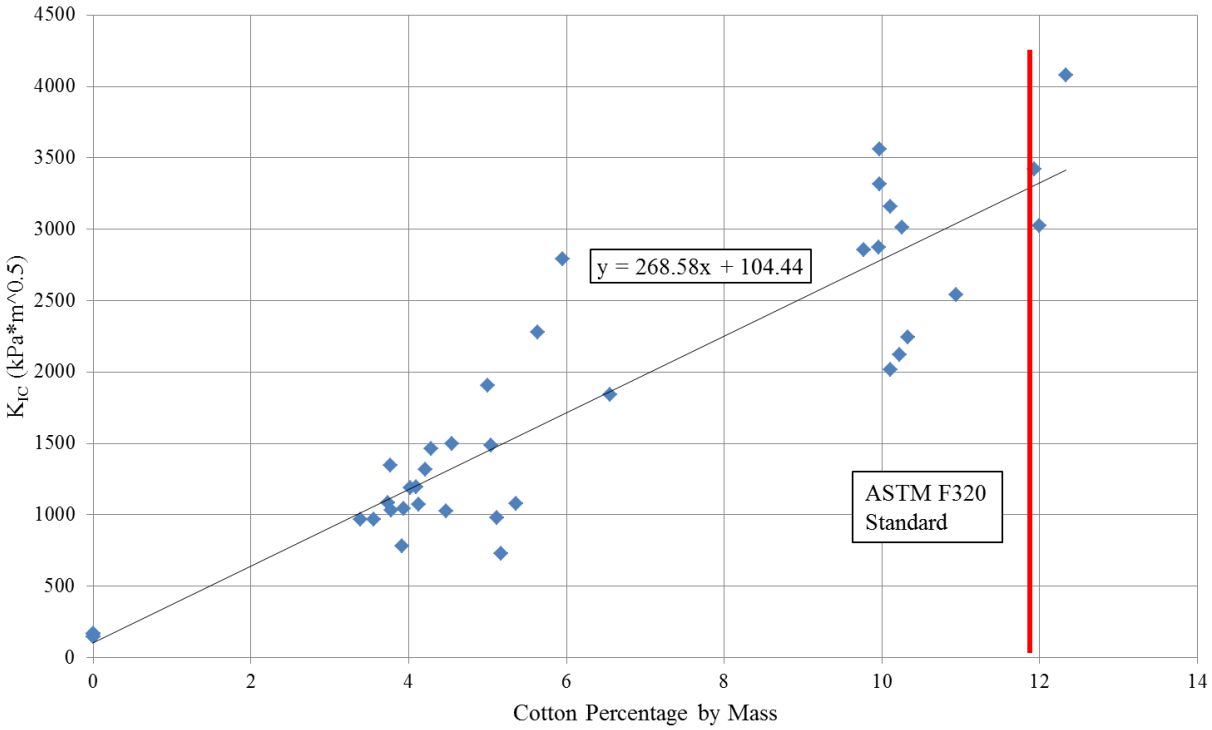

Figure 35: K_{IC} Relationship to Cotton Percentage by Mass, with Trendline

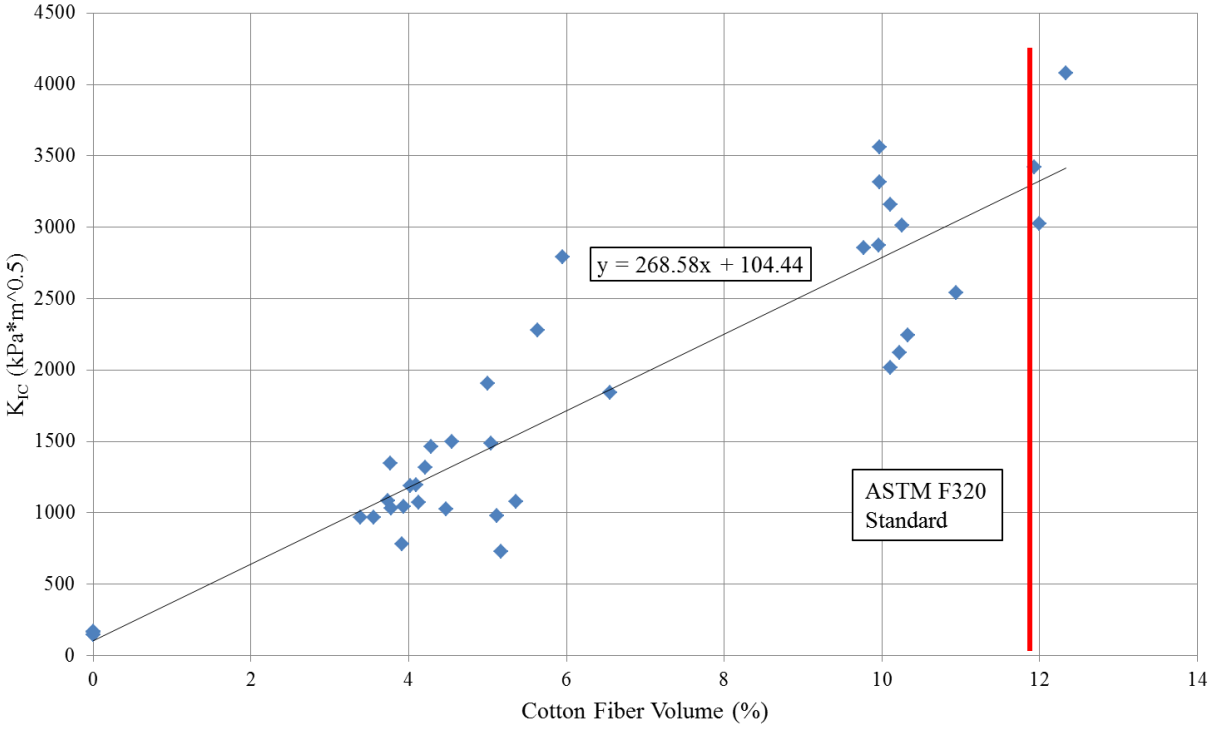

Figure 36: K_{IC} Relationship to Cotton Fiber Volume, with Trendline

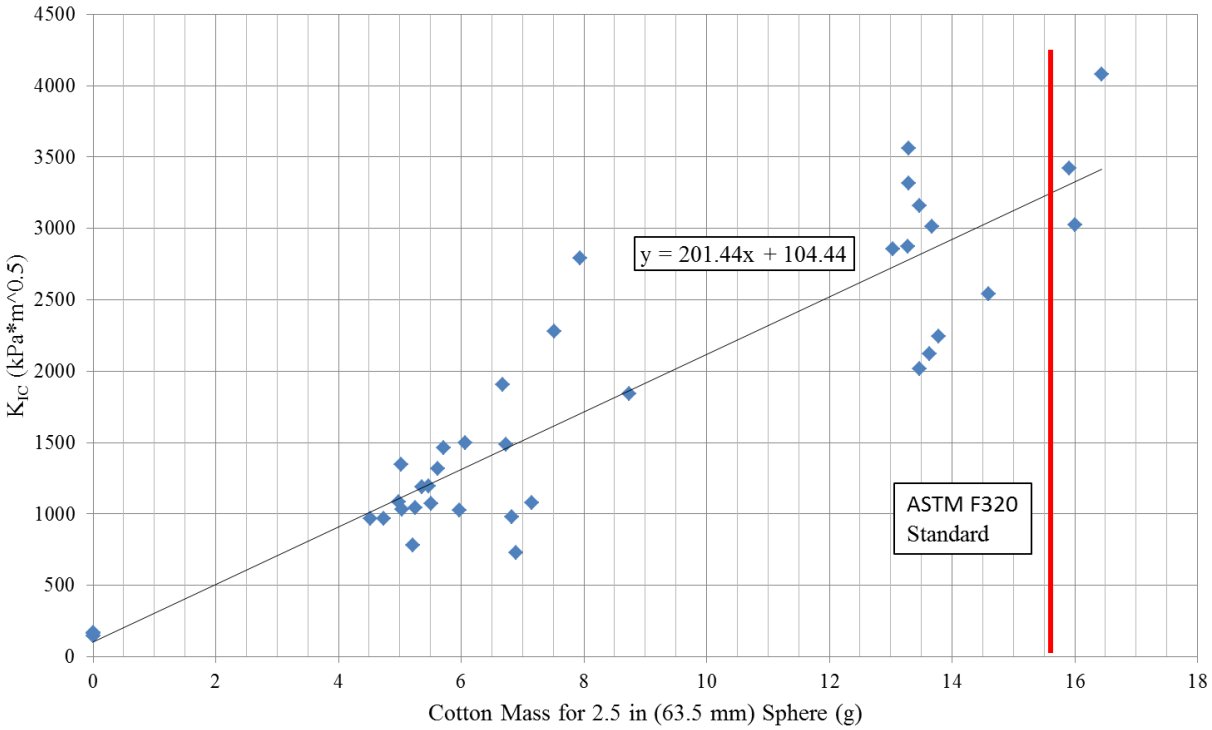

Figure 37: K_{IC} Relationship to Cotton Mass for 2.5 in (63.5 mm) Sphere, with Trendline

3. Conclusions

There are several important conclusions which can be drawn from this data. First, it is possible to approximate cold room experimental results in a warm room test environment. This can be done by decreasing the time from when each specimen is pulled out of the freezer to when it is tested and by using insulation, such as styrofoam pads, to thermally isolate each specimen from the testing equipment.

Most important, at quasi static speeds there is an approximately linear relationship between cotton concentration and the critical K_I value. This relationship is described by the equation

$$K_{IC} = 268.584ct_p + 104.44 \tag{5}$$

where ct_p is the amount of cotton in the specimen as a percentage of the total mass. The fracture toughness increases because cotton restricts crack propagation. More energy is required to separate the ice from the fiber threads than to crack clear ice.

This also suggests that the fracture toughness is limited by the amount of cotton which can be physically present in a sample. This testing demonstrated that it is difficult to precisely control the cotton concentration using the described manufacturing method. The actual concentration could only be determined after testing had been completed. Likewise, it would be difficult to increase the cotton concentration above the ASTM F320 standard of 12% cotton by mass without using a pressurized mold.

E. Compression Strength

As mentioned previously, literature and previous research has indicated that fracture toughness and compression strength are the dominant factors of the failure mode of SHI. Though estimates were made of the compression and tensile strength of clear and cotton-SHI using spherical test data, it was important to determine the actual compression strength of the clear and cotton reinforced ice. The method chosen was to crush cylinders of constant cross section at a known crosshead displacement rate.

1. Test Description and Procedure

The first step in the experiment was to reproduce the results from other compression tests found in literature. Test specimens were prepared the same as the fracture toughness samples without the notch. Several samples were trimmed to $3 \times 1.5 \times 1.5$ in ($80 \times 40 \times 40$ mm), though most were trimmed to $1.5 \times 1.5 \times 1.5$ in ($40 \times 40 \times 40$ mm) after it was determined that the sample height did not significantly affect the compression strength results. Styrofoam insulation end caps were placed in between the specimens and the rigid aluminum plates. Any imperfection in the surface of the ice could create a local stress concentration, causing local cracking and premature failure. Each end cap was cut to $1.5 \times 1.5 \times 0.25$ in ($40 \times 40 \times 7$ mm), and was used only once during testing. A picture of the setup is shown in Figure 38.

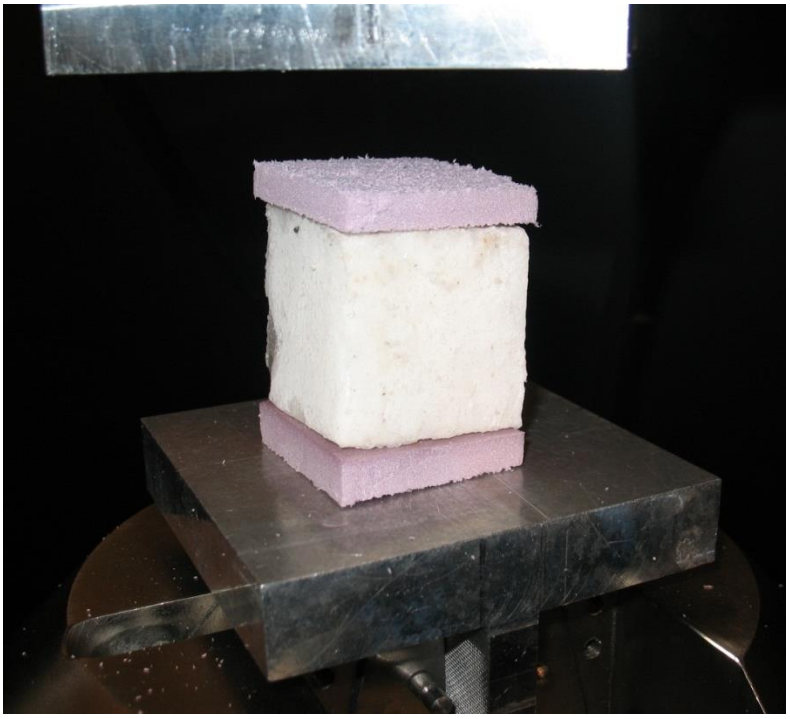

Figure 38: Compression Test Setup

All compression strength tests were performed on an Instron 8801 machine at a strain rate of 0.4 1/s. The machine setup and basic test procedures were identical to the sphere crush tests. Because the specimens were not in direct contact with the aluminum platens, no effort was made to keep the platens cold.

Even though the cubes were stored at 7°F (-22°C), the cubes would begin to warm once removed from the freezer. Using the normal test procedures, the cube would have warmed to 17°F (-8°C) by the time the test began, as shown in Figure 39, with some additional warming along the edges. The styrofoam caps effectively isolate the specimens thermally from the test equipment, as can be seen by the thermal gradient.

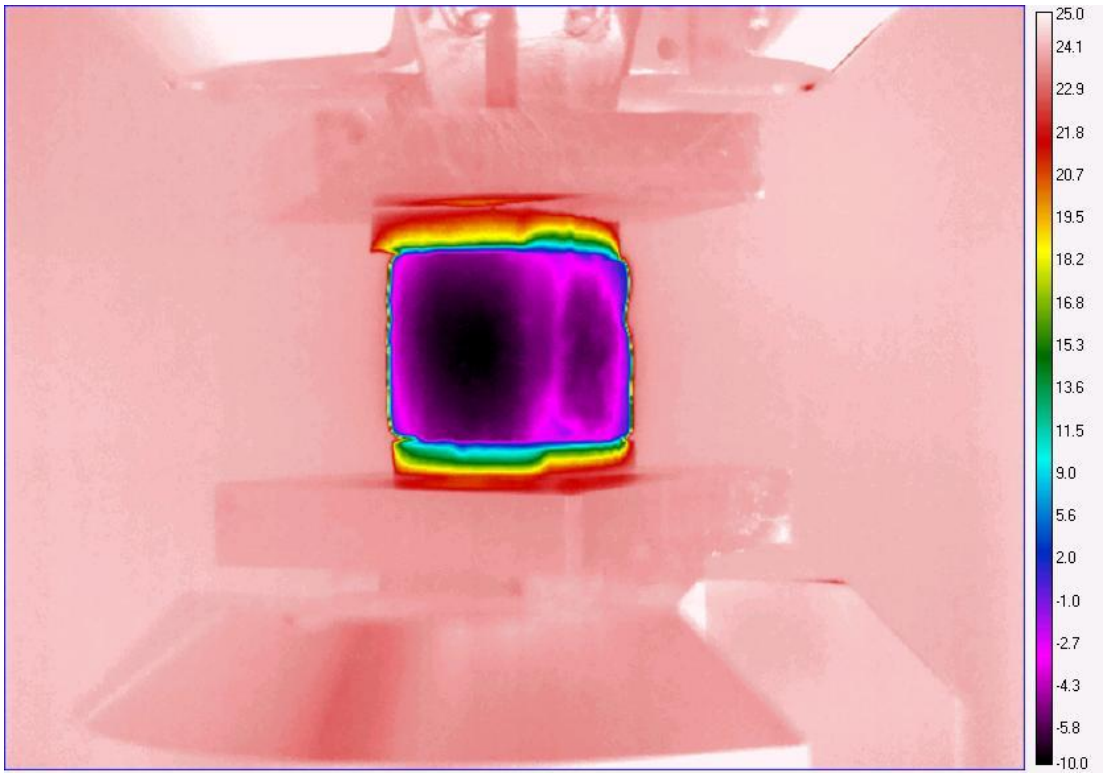

Figure 39: Cube Thermal Picture, Pre-Fracture

2. Data Reduction and Analysis

The clear ice compression strength data is shown in Figure 40 overlaid with the data reproduced from Kim and Keune [20]. It can be seen, using this method, the clear ice compression strength data agrees relatively well with other researchers. Further improvements could be made to the samples to help control imperfections in the ice, but this was considered unnecessary as hail is not a perfectly controlled material.

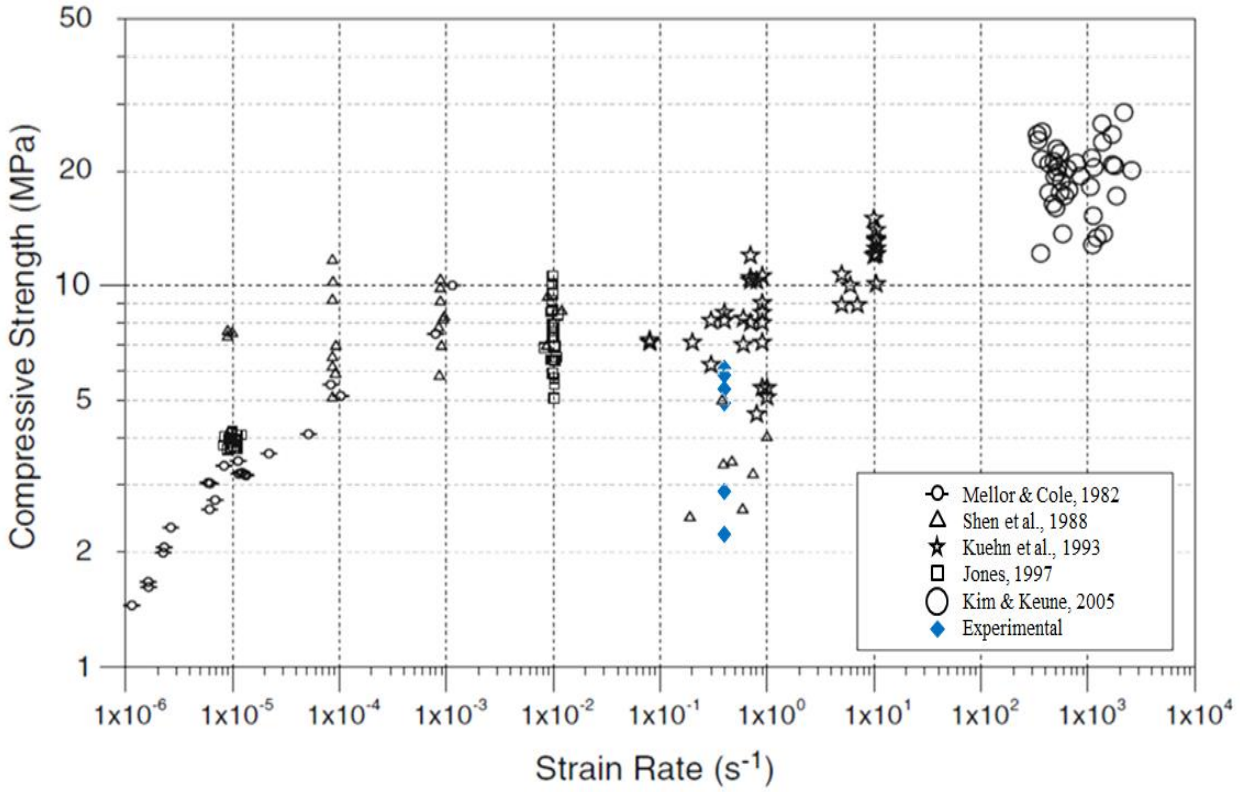

Figure 40: Clear Ice Compression Strength Literature Comparison

The results of the compression strength tests as a function of cotton content are shown in Figure 41 through Figure 43. The charts show the same type of data, one in terms of the cotton percentage, one in terms of fiber volume, and the third in terms of the equivalent amount of cotton in a 2.5 in (63.5 mm) sphere.

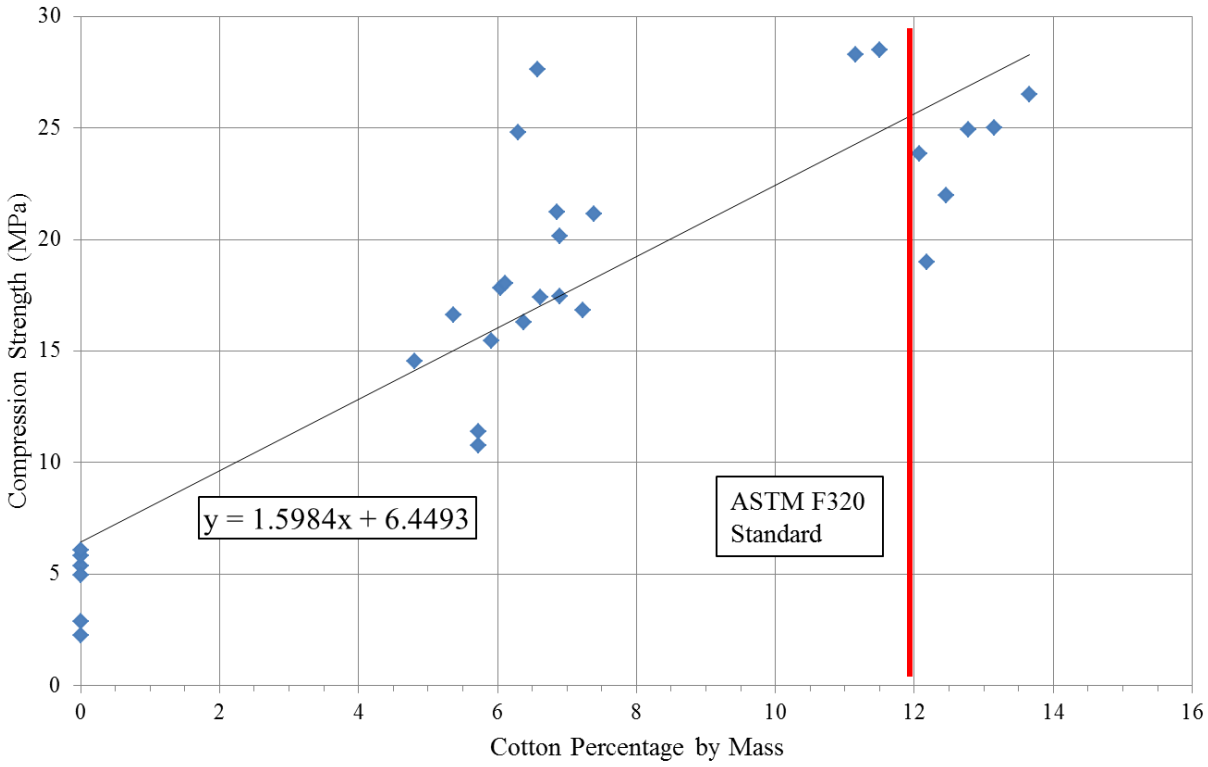

Figure 41: Compression Strength Relationship to Cotton Percentage by Mass, with Trendline

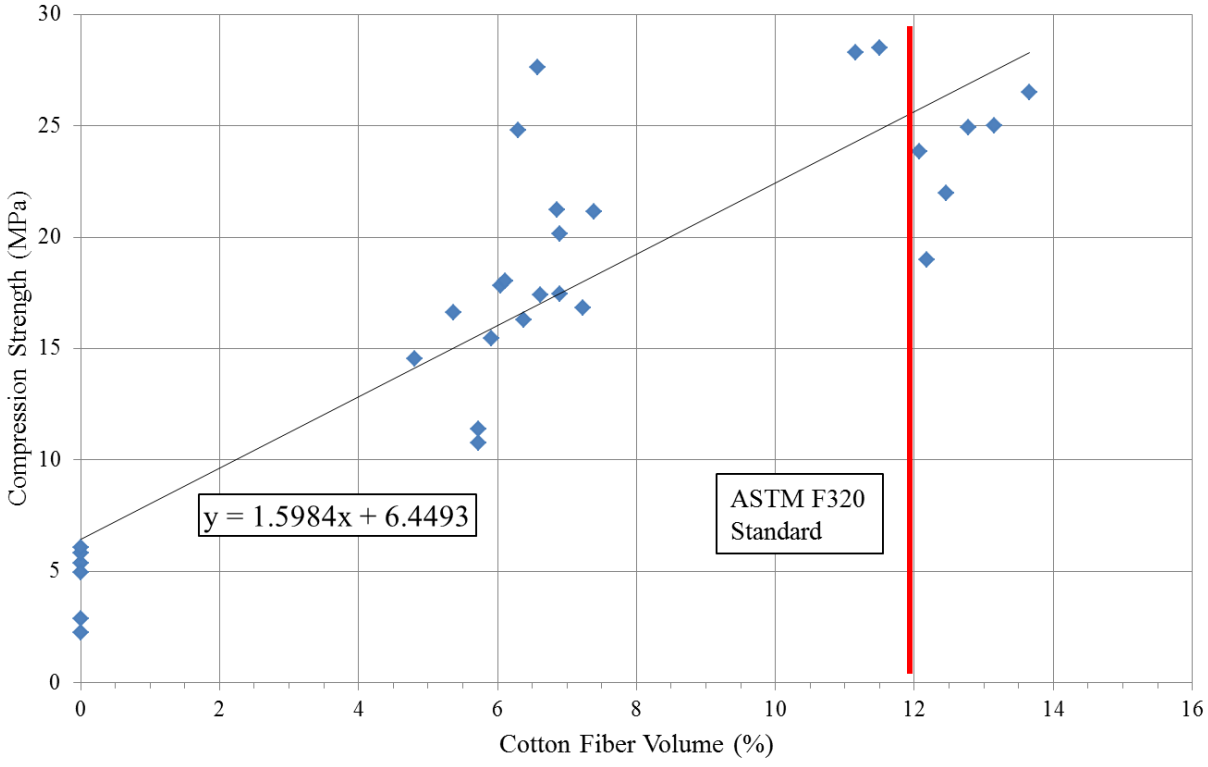

Figure 42: Compression Strength Relationship to Cotton Fiber Volume, with Trendline

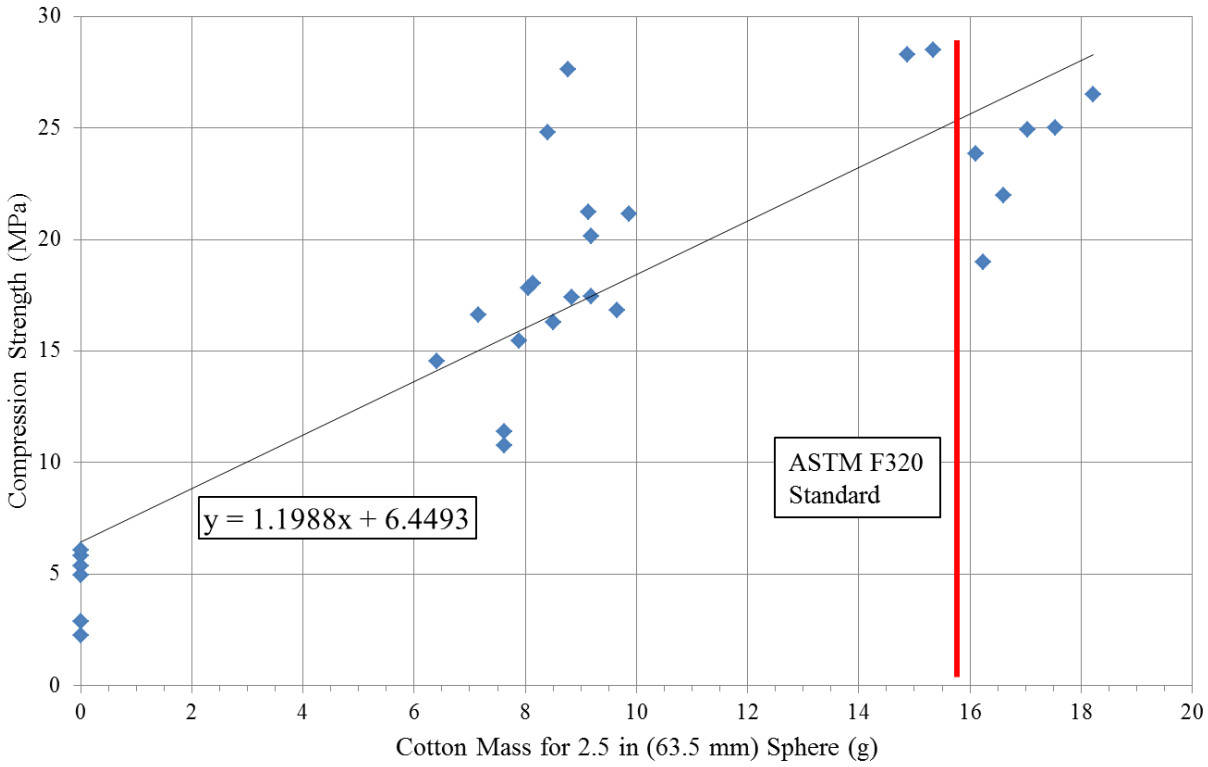

Figure 43: Compression Strength Relationship to Cotton Mass for 2.5 in Sphere, with Trendline

There are several important conclusions which can be made about this data. As can be seen in Figure 41 through Figure 43, like fracture toughness, compression strength has an approximately linear relationship with the cotton concentration. This relationship is described by the equation

$$\sigma_c = 1.5984 ct_p + 6.4493 \quad (6)$$

where ct_p is the amount of cotton in the specimen as a percentage of the total mass. This suggests that the cotton fibers are carrying the load in the specimen. The concept is analogous to increasing the fiber volume content in a composite fiber-matrix material. Due to the variability in the clear and cotton-ice samples, it is recommended that any future testing use at least six samples per concentration.

Another important conclusion can be made from how differently the clear and cotton ice samples failed, as shown in Figure 44. The clear ice samples tended to fail catastrophically. Once the first cracks developed, the cracks spread uncontrollably resulting in a massive release of energy. This energy caused the samples to break apart into many small fragments. If uncontained, some ice shards traveled up to about 15 ft (4.5 m) away from the test machine. In contrast, the cotton-ice samples failed either by flattening into a disc or several large pieces partially held together by the cotton fibers. As in the fracture toughness tests, cotton holds the ice together after fracture. The ice may be broken, but the combination of fibers and ice transfer the compression loads, increasing the overall strength of the material.

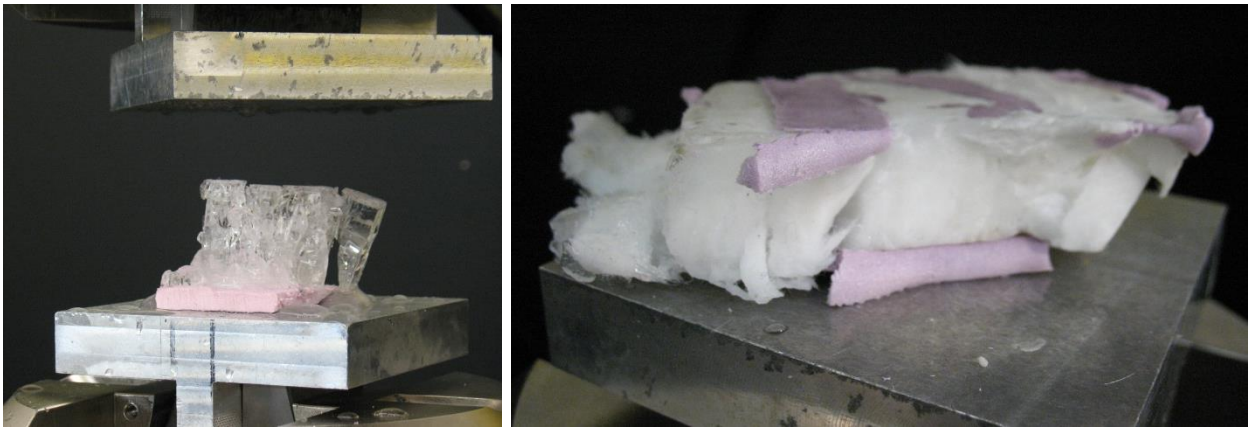

Figure 44: Clear and Cotton Cube Specimens, Post-Fracture

V. Conclusions

Hail is a significant threat to aircraft which can severely damage an aircraft in flight and on the ground. To improve safety and decrease maintenance and repair costs, aircraft need to be designed to mitigate this weather threat. Unfortunately, the mechanical properties of hail are not well understood. It is difficult to obtain natural hailstones suitable for testing. Most research has focused on either assuming that hail can be represented by solid ice, or that some form of fiber additive is necessary to better represent the presumably greater toughness of hail over ice. It is important to note that data is readily available for clear but not cotton fiber reinforced ice.

To cover both assumptions, tests were done to determine the mechanical properties of both clear and cotton fiber reinforced Simulated Hail Ice (SHI). Photographs were taken of the internal crystal structure of the SHI. It was discovered that the SHI may be considered isotropic and that cracks may form across grain boundaries. The force-displacement crush curves of spherical SHI were characterized. The compression strength and fracture toughness of clear and cotton fiber reinforced ice was also characterized at various strain rates. There is a linear relationship between the amount of cotton and both the compression strength and fracture toughness. This suggests that the fibers carry the load within the SHI in much the same way composite materials behave. It was shown that it is possible to approximate cold room experimental results in a warm room test environment if the proper care was taken to thermally isolate the specimens from the testing equipment.

High speed photography was used to document the failure mechanism, suggesting that SHI fails through a combination of compression failure followed by tensile fracture. When under compression, SHI experiences a region of compression near the point of impact and

tension throughout the center of the sphere. As the load increases, cracks propagate away from the point of impact, limited by the compression strength of the SHI. When the cracks reach the tensile region, the fracture toughness of the SHI governs the catastrophic fracture. For clear-SHI, failure generally occurs through the propagation of one or two cracks. However, failure within cotton-SHI tends to occur when several separately formed cracks interact, though the cotton fibers may continue to carry an increasingly smaller load. Thus, the compression strength and fracture toughness results can be used to describe the spherical SHI crush test results.

For future research, it recommended that the strength and toughness of both clear and cotton-SHI be determined at higher strain rates. When the mechanical properties of hail are actually tested, this data can then be refined to best approximate the natural impact behavior.

References

1. Field, P. R., et al. *Hail Threat Standardisation*. Research rept. no. 2008/5. N.p.: European Aviation Safety Agency, 2010. Print, p 13.
2. Noon, Randall K. "Ch 21: Hail Damage." *Forensic Engineering Investigation*. N.p.: CRC, 2000. N. pag. Print.
3. Court, Arnold, and John F. Griffiths. "Thunderstorm Climatology." *Thunderstorm Morphology and Dynamics*. Ed. Edwin Kessler. 2nd ed. Norman: U of Oklahoma, 1986. 9-39. Print. Vol. 2 of *Thunderstorms: A Social, Scientific, and Technological Documentary*. 3 vols, p 36.
4. NTSB Identification: DCA98MA045. *National Transportation and Safety Board*. N.p., n.d. Web. 13 Feb. 2013. <http://www.ntsb.gov/aviationquery/brief.aspx?ev_id=20001211X10040&key=1>.
5. *AirTran Flight 426 - Crushing Hail, Shattered Windows, No Instruments*. *Youtube*. N.p., n.d. Web. 13 Feb. 2013. <http://www.youtube.com/watch?v=nxaK837lebk>.
6. ASN Aircraft Accident Boeing 737-33V HB-III Oyonnax. *Aviation Safety Network*. Flight Safety Foundation, n.d. Web. 13 Feb. 2013. <http://aviation-safety.net/database/record.php?id=20030815-0>.
7. Field, P. R., et al. *Hail Threat Standardisation*. Research rept. no. 2008/5. N.p.: European Aviation Safety Agency, 2010. Print, p 109.
8. "Tornado Damage Cancels Hundreds of Flights from Dallas-Fort Worth." *NBC News*. N.p., n.d. Web. 13 Feb. 2013. <http://www.nbcnews.com/travel/tornado-damage-cancels-hundreds-flights-dallas-fort-worth-650594>.
9. Fourth Quarter 2006. *Aero Magazine*. Boeing, n.d. Web. 13 Feb. 2013. <http://www.boeing.com/commercial/aeromagazine/articles/qtr_4_06/>.
10. Vogelaar, Rob. "A350 XWB First Composite Lay-Up Manufactured in Nantes." *Aviation News*. N.p., 4 Dec. 2009. Web. 13 Feb. 2013. <http://www.aviationnews.eu/2009/12/04/a350-xwb-first-composite-lay-up-manufactured-in-nantes/>.
11. U.S. Department of Transportation. Federal Aviation Administration. *Pilot's Handbook of Aeronautical Knowledge*. Rept. no. FAA-H-8083-25A. Oklahoma City: n.p., 2008. Print, p7-8.

12. 14 C.F.R. Sec. 25.571. 2013. Print.
13. 14 C.F.R. Sec. 25.773. 2013. Print.
14. *Standard Test Method for Hail Impact Resistance of Aerospace Transparent Enclosures*. Rept. no. F320-10. N.p.: ASTM International, 2010. Print.
15. Schulson, Erland M. "The Structure and Mechanical Behaviour of Ice." JOM (1999): 21-27. Print, p 21-22.
16. Ibid. p 23.
17. Schulson, Erland M., and Paul Duval. "Physical Properties: Elasticity, Friction and Diffusivity." *Creep and Fracture of Ice*. N.p.: Cambridge UP, 2009. 51-76. Print, p 59.
18. Field, P. R., et al. *Hail Threat Standardisation*. Research rept. no. 2008/5. N.p.: European Aviation Safety Agency, 2010. Print, p 14.
19. Schulson, Erland M., and Paul Duval. "Ductile Behavior of Polycrystalline Ice: Experimental Data and Physical Processes." *Creep and Fracture of Ice*. N.p.: Cambridge UP, 2009. 101-152. Print.
20. Schulson, Erland M., and Paul Duval. "Brittle Failure of Ice Under Tension." *Creep and Fracture of Ice*. N.p.: Cambridge UP, 2009. 212-235. Print, p 217-18.
21. Kim, Hyonny, and John N. Keune. "Compressive Strength of Ice at Impact Strain Rates." *Journal of Material Science* 42 (2007): p2802-06. Print.
22. Schulson, Erland M., and Paul Duval. "Brittle Compressive Failure of Unconfined Ice." *Creep and Fracture of Ice*. N.p.: Cambridge UP, 2009. 236-265. Print, p 237-39.
23. Shazly, Mostafa, Vikas Prakash, and Bradley A. Lerch. *High-strain-rate Compression Testing of Ice*. Cleveland, Ohio: National Aeronautics and Space Administration, Glenn Research Center, 2006. Internet resource.
24. Schulson, Erland M., and Paul Duval. "Brittle Failure of Ice Under Tension." *Creep and Fracture of Ice*. N.p.: Cambridge UP, 2009. 212-235. Print, p 213-14.
25. Schulson, Erland M., and Paul Duval. "Fracture Toughness of Ice." *Creep and Fracture of Ice*. N.p.: Cambridge UP, 2009. 190-211. Print, p 193
26. Schulson, Erland M., and Paul Duval. "Fracture Toughness of Ice." *Creep and Fracture of Ice*. N.p.: Cambridge UP, 2009. 190-211. Print, p 198-99.
27. Nixon, W A, and E M. Schulson. "A Micromechanical View of the Fracture Toughness of Ice." Le Journal De Physique Colloques. 48 (1987). Print.

28. Schulson, Erland M., and Paul Duval. "Fracture Toughness of Ice." *Creep and Fracture of Ice*. N.p.: Cambridge UP, 2009. 190-211. Print, p 202-03.
29. Field, P. R., et al. *Hail Threat Standardisation*. Research rept. no. 2008/5. N.p.: European Aviation Safety Agency, 2010. Print, p 16.
30. Hiramatsu, Y., and Y. Oka. "Determination of the Tensile Strength of Rock by a Compression Test of an Irregular Test Piece." *International Journal of Rock Mechanics and Mining Sciences* 3 (1966): p89-99. Print.
31. Darvell, B. W. "Uniaxial Compression Tests and the Validity of Indirect Tensile Strength." Journal of Materials Science 25 (1990): p757-80. Print.
32. Chau, K.T, X.X Wei, R.H.C Wong, and T.X Yu. "Fragmentation of Brittle Spheres Under Static and Dynamic Compressions: Experiments and Analyses." *Mechanics of Materials*. 32.9 (2000): p543-554. Print.
33. Wu, S.Z, K.T Chau, and T.X Yu. "Crushing and Fragmentation of Brittle Spheres Under Double Impact Test." *Powder Technology*. (2004): p41-55. Print.
34. Luscher, W.G, J.R Hellmann, A.E Segall, D.L Shelleman, and B.E Scheetz. "A Critical Review of the Diametral Compression Method for Determining the Tensile Strength of Spherical Aggregates." *Journal of Testing and Evaluation*. 35.6 (2007): p624-629. Print.
35. Russell, Adrian R., and David Muir Wood. "Point Load Tests and Strength Measurements for Brittle Spheres." *International Journal of Rock Mechanics and Mining Sciences* 46 (2009): p272-80. Print.
36. Marquardt, Oliver. "Tests and Simulations of Simulated Hail Ice at Quasi-Static Damage Velocities." MS thesis. U of Stuttgart, 2012. Print.
37. Murakami, Y. Stress Intensity Factors Handbook. Oxford: Pergamon, 1987. Print.

Appendix

A. Appendix A: Raw 2.5 in (63.5mm) Test Data, "Slow" Strain Rate = 0.01 1/s

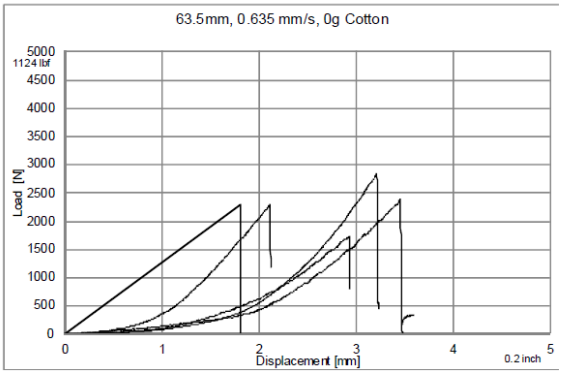

(a) 2.5"/clear SHI

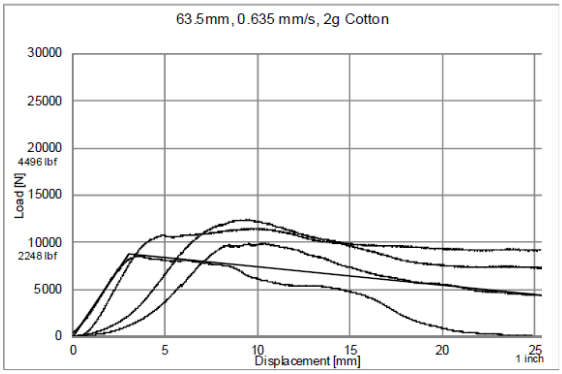

(b) 2.5"/2g SHI

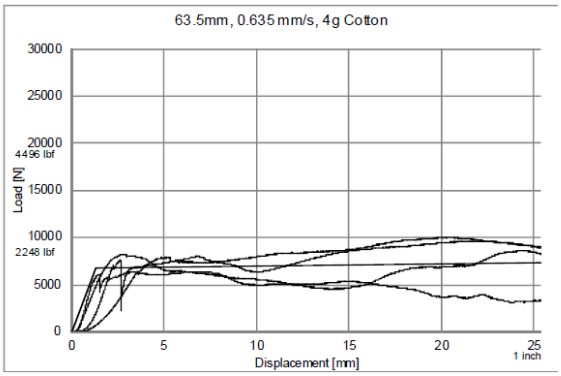

(c) 2.5"/4g SHI

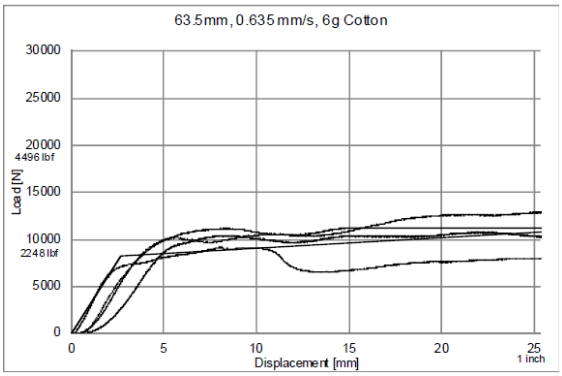

(d) 2.5"/6g SHI

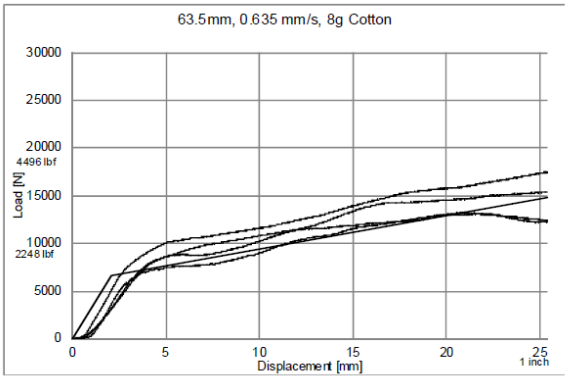

(e) 2.5"/8g SHI

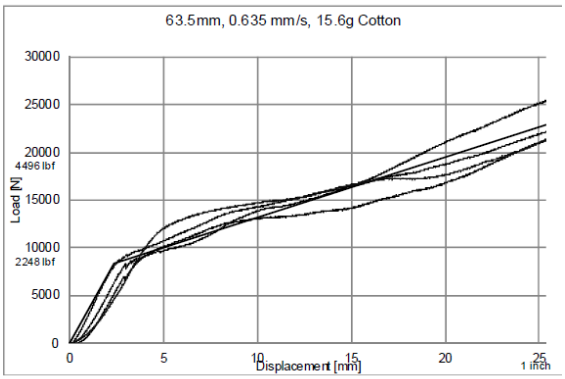

(f) 2.5"/15.6g SHI

B. Appendix B: Raw 2.5 in (63.5mm) Test Data, "Fast" Strain Rate = 0.4 1/s

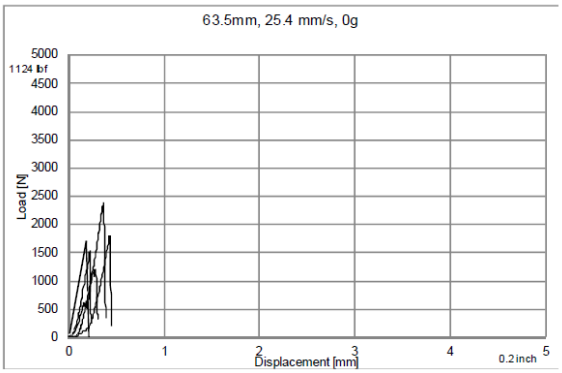

(a) 2.5"/clear SHI

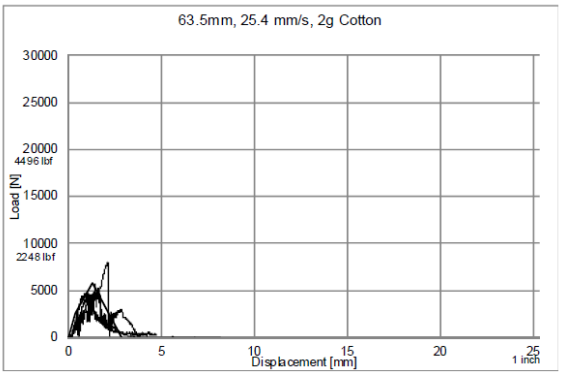

(b) 2.5"/2g SHI

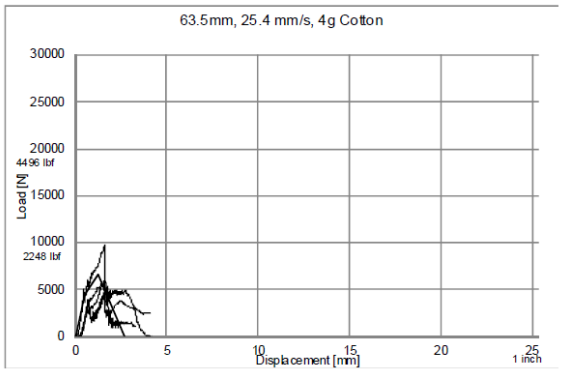

(c) 2.5"/4g SHI

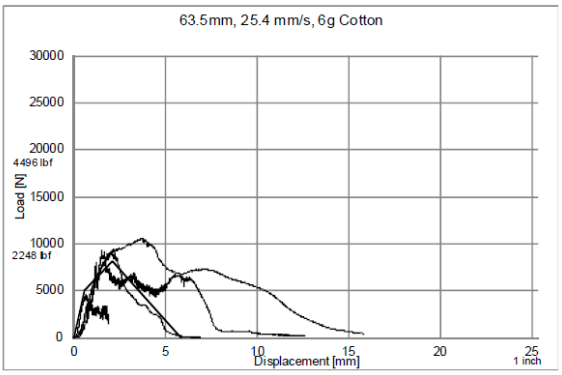

(d) 2.5"/6g SHI

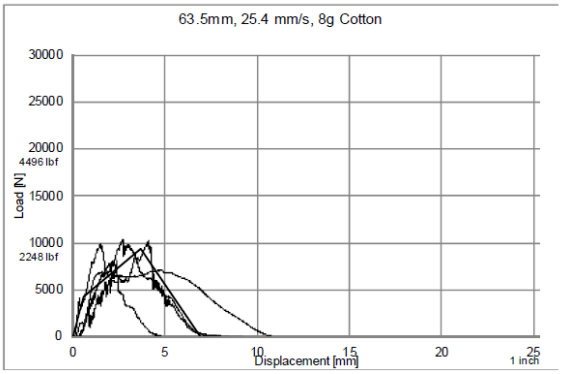

(e) 2.5"/8g SHI

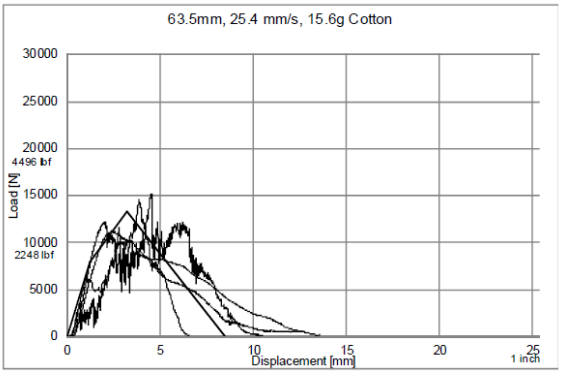

(f) 2.5"/15.6g SHI

Acknowledgements

This Thesis Report and Project could not have been completed without the grateful assistance of many people, including:

- Dr. Paolo Feraboli, advisor and mentor for my project. I am grateful to him for accepting me as a student at the Advanced Composite Structures Laboratory (ACSL), pushing me to be a better researcher, and making this a valuable and memorable experience.
- The Staff of the ACSL, in particular Bonnie Wade and Max Spetzler. They helped me refine my project, kept me pointed in the right direction, and gave me much needed advice, support, and encouragement.
- Oliver Marquadt, for beginning the project and collecting data, in particular as relates to the spherical SHI crush tests.
- Robert Gordon and Jack Ross, for their assistance in helping me set up and troubleshoot the experiments and equipment.
- Wanda Frederick, for helping me come to the University of Washington in the first place.
- Barrett McCann, Lieutenant Colonel, U.S. Air Force and Alyssa Tetrault, Captain, U.S. Air Force, my Air Force Institute of Technology (AFIT) Liaison Officer and Program Manager, respectively, for their support.
- My family, parents Michael and Shelly, and siblings Jennifer, Jessica, Jordan, and Jared. I could not have made it through the program without you.

Disclaimer: The views expressed in this thesis are those of the author and do not reflect the official policy or position of the United States Air Force, Department of Defense, or the U.S. Government.